UNIVERSITÀ DEGLI STUDI DI TORINO

Doctoral School in Life and Health Sciences

PhD in Medical Pathophysiology

Cycle XXXVI

PhD THESIS

Validation of Extracellular Vesicles expressing SARS-CoV-2 Spike protein (S-EVs) as a model of virus like particle for possible theragnostic applications

Scientific Supervisor

Prof. Benedetta Bussolati

PhD Student

Dr. Roberta Verta

Academic year 2023-2024

Index

ABSTRACT

Coronavirus disease 2019 (COVID-19), caused by the highly contagious severe acute respiratory syndrome coronavirus 2 (SARS-CoV-2), has had a devastating global impact, leading to the loss of over 6 million lives worldwide [1],[2]. A key factor for the SARS-CoV-2 virus infection is the binding between the spike protein (S) of virus and the angiotensin converting enzyme 2 (ACE2) receptor, present on the membrane of the target cells [3]. The S protein is characterized by two different functional subunits, the S1 and S2. In particular, S1 mediates the specific ACE2 interaction, while S2 the fusogenic properties of the S protein and is responsible for the virus internalization [4],[5].

Extracellular vesicles (EVs) are considerably similar to viruses in terms of size, structure, biogenesis, ability to transport small nucleic acids and ability to enter in target cells [6]. Recently, it was demonstrated that exosomes from infected cells can contain viral material or whole viral particles facilitating the virus spread and infection [7]. The use of viral elements and EV properties it is of great interest, especially considering the absence of specific anti-viral therapies to contrast SARS-CoV-2 infection.

Therefore, the aim of this work was to generate a simple, safe, and scalable model to study therapeutic approaches against SARS-CoV-2 infection, such as block of the cell binding and of virus internalization, through the analysis of EV properties. For this purpose, we collected EVs from human embryonic kidney cells (HEK-293T) previously transfected with mammalian expression vector coding for the S protein (H-S), obtaining EVs expressing S protein (S-EVs) with diameter between 50-100nm, size assessed by TEM and nanoparticle tracking analysis (NTA). S-EVs were widely characterized using western blot, MACSPlex, ExoVieW and super resolution microscopy. The spike on EV surface co-expressed with hallmark exosome marker tetraspanins (CD9, CD63, CD81).

Using super-resolution microscopy and MACSPlex analyses, we identified the presence of different subpopulations of S-EVs. The S-EVs were either positive for both the subunits (S1S2-EVs), only for S1 (S1-EVs) or for S2 (S2-EVs). Subsequently, we analyzed the EV-cell interaction using supported lipid bilayer, cell membrane model, where we observed a major area of interaction and membrane perturbation after the S-EV addition in respect to the EVs without the spike protein.

Once demonstrated the EV interaction with the cell membrane model, we compared the S-EV uptake capability between ACE2 positive (HUVEC, 16HBE14o-) and negative cells (G7, HK-2) in order to validate the specificity of S-ACE2 receptor interaction. The cytofluorimetric analysis showed that S-EVs were significantly more internalized by ACE2 positive cells in respect to the EVs without spike, control EVs. In contrast, we observed a significative increase in the uptake of control EVs (C-EVs) in ACE2 negative cells. These results were further confirmed by the treatment with anti-ACE2 blocking antibody that significantly inhibited exclusively the S-EV uptake by HUVEC e 16HBE14o- cells.

Finally, to investigate new possible therapeutic solutions against SARS-CoV-2 infection, we evaluated the effect of colchicine, a microtubule antagonist and anti-inflammatory drug, used in clinical trials on COVID19, on S-EV uptake modulation. Colchicine was able to significantly reduce the EV uptake in target cells, independently of spike protein presence.

This inhibitory effect of colchicine prompted us to study its potential role in the EV uptake inhibition of EVs from ovarian adenocarcinoma (SKOV3) and colorectal cancer (HT29) cells. The SKOV3-EV and HT29-EV cell entrance were assessed. We observed a significant reduction in tumor-EV uptake by endothelial cells after colchicine treatment, both using physiological endothelium (HMEC) and endothelial cancer cells (EcK).

In conclusion, we demonstrated the possibility to generate EVs, expressing on their surface the SARS-CoV-2 spike protein (S-EVs), from HEK-293T-spike transfected cells, as a model to study the virus and host cell interaction. S1-EVs could be useful for diagnostic purposes thanks to specific ACE2expression, whereas S1S2-EVs could be employed for drug delivery to target cells (ACE2 positive). These results open the door to new future scenarios in theragnostic applications, allowing to overcome the problems related to the endosomal degradation of EVs which represent a potential limit for EV-based therapies. Finally, we identified a new pharmacological tool to modulate EV entry, that deserves further studies for possible application not only in SARS-CoV2, but also in oncology.

SARS-CoV-2 and COVID-19

Novel Coronavirus

Severe acute respiratory syndrome coronavirus 2 (SARS-CoV-2) is a highly transmissible and pathogenic coronavirus that emerged in late 2019 and responsible of pandemic of acute respiratory disease, called ‘coronavirus disease 2019’ (COVID-19) with its unprecedented global human health, social and economic impact [8],[9]. Coronaviruses (CoVs) are a family of enveloped positive-sense single-stranded RNA viruses. They infect humans, other mammals and avian species, including livestock and companion animals, and are therefore not only a challenge for public health but also a veterinary and economic concern. Human coronaviruses, such as HCoV-229E and HCoV-OC43, have long been known to circulate in the population and they, together with the more recently identified HCoV-NL63 and HCoV-HKU1, cause seasonal and usually mild respiratory tract infections associated with symptoms of the ‘common cold’ [8]. Instead, severe acute respiratory syndrome coronavirus (SARS-CoV), Middle East respiratory syndrome coronavirus (MERS-CoV) and SARS-CoV-2 are highly pathogenic. By infecting bronchial epithelial cells, pneumocytes and upper respiratory tract cells in humans, SARS-CoV, MERS-CoV and SARS-CoV-2 infections can develop into severe, life-threatening respiratory pathologies and lung injuries for which no specific therapeutic treatment has been approved [10]. Clinical manifestations of COVID-19 patients range from dyspnea, fever, cough, and headache to severe cases of pneumonia that can lead to death [11].

SARS-CoV-2 characteristics

The SARS-CoV-2 genome sequence shares approximately 80% sequence identity with SARS-CoV and 50% with MERS-CoV. Its genome comprises 14 open reading frames (ORFs), which encode 16 nonstructural proteins (nsp 1–16) that make up the replicase complex and 9 accessory proteins (ORF) and 4 structural proteins: spike (S), envelope (E), membrane (M), and nucleocapsid (N). S mediates SARS-CoV entry into host cells [12]. However, the S gene of SARS-CoV-2 is extremely variable from SARS-CoV, with minus of 75% nucleotide identity. S possess a receptor-binding domain (RBD) that mediates direct contact with a cellular receptor, angiotensin-converting enzyme 2 (ACE2) present on the virus target cells, and an S1/S2 polybasic cleavage site that is proteolytically cleaved by cellular cathepsin L and the transmembrane protease serine 2 (TMPRSS2). TMPRSS2 facilitates viral entry at the plasma membrane surface, while cathepsin L activates SARS-CoV-2 S in endosomes and can compensate for entry into cells that lack TMPRSS2 [13] (Fig. 1). Once the genome is released into the host cytosol, ORF1a and ORF1b are translated into viral replicase proteins, which are cleaved into individual non-structural proteins (NPSs) (via host and viral proteases: PLpro); these form the RNA-dependent RNA polymerase (NSP12 derived from ORF1b) [12]. Here, the replicase components rearrange the endoplasmic reticulum (ER) into double-membrane vesicles (DMVs) that facilitate viral replication of genomic and subgenomic RNAs (sgRNA); these are translated into accessory and viral structural proteins for the virus particle formation [14] (Fig. 1).

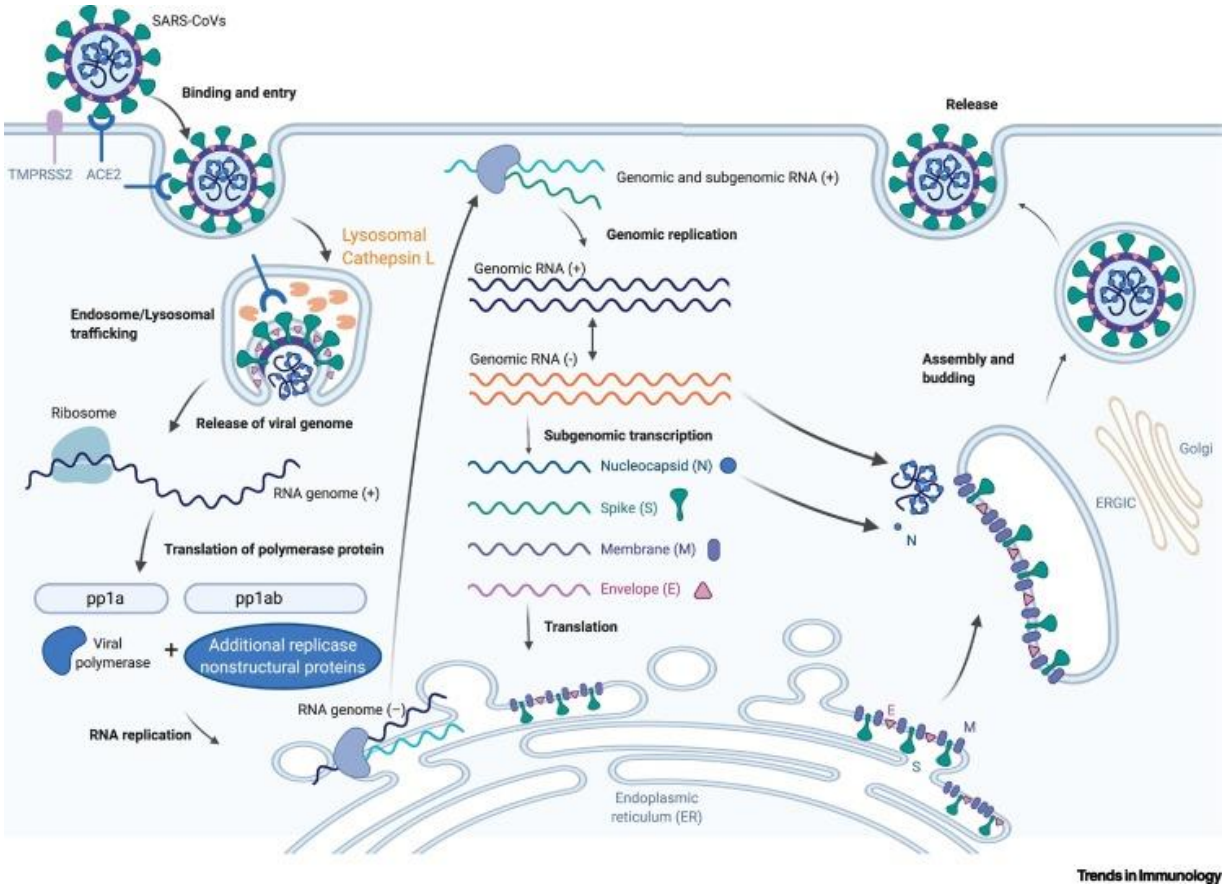

Figure 1. The Severe Acute Respiratory Syndrome Coronavirus 2 (SARS-CoV-2) Lifecycle. The SARS-related coronavirus (SARS-CoV and SARS-CoV-2) lifecycle commences by binding of the envelope Spike protein to its cognate receptor, angiotensin-converting enzyme 2 (ACE2). Efficient host cell entry then depends
on: (i) cleavage of the S1/S2 site by the surface transmembrane protease serine 2 (TMPRSS2); and/or (ii) endolysosomal cathepsin L, which mediate virus–cell membrane fusion at the cell surface and endosomal compartments, respectively. Through either entry mechanism, the RNA genome is released into the cytosol, where it is translated into the replicase proteins (open reading frame 1a/b: ORF1a/b). The polyproteins (pp1a and pp1b) are cleaved by a virus-encoded protease into individual replicase complex nonstructural proteins (nsps) (including the RNA-dependent RNA polymerase: RdRp). Replication begins in virus-induced doublemembrane vesicles (DMVs) derived from the endoplasmic reticulum (ER), which ultimately integrate to form elaborate webs of convoluted membranes. Here, the incoming positive-strand genome then serves as a template for full-length negative-strand RNA and subgenomic (sg)RNA. sgRNA translation results in both structural proteins and accessory proteins (simplified here as N, S, M, and E) that are inserted into the ER–Golgi intermediate compartment (ERGIC) for virion assembly. Finally, subsequent positive-sense RNA genomes are incorporated into newly synthesized virions, which are secreted from the plasma membrane. Figure from Harrison, Andrew G et al. “Mechanisms of SARS-CoV-2 Transmission and Pathogenesis.” Trends in immunology vol. 41,12 (2020): 1100-1115. doi:10.1016/j.it.2020.10.004.

The SARS-CoV-2 Spike glycoprotein

The initial steps of coronavirus infection involve the specific binding of the coronavirus S protein to the cellular entry receptors. Coronavirus S proteins is homotrimeric class I fusion glycoprotein divided into two functionally distinct parts, S1 and S2. The S1

subunit of a coronavirus is further divided into two functional domains, an N-terminal domain and a C-terminal domain. Structural and biochemical analyses identified a 211 amino acid region (amino acids 319–529) at the S1 C-terminal domain of SARS-CoV-2 as the receptor-binding domain (RBD), which has a key role in virus entry. Biochemical data demonstrated that the structural features of the SARS-CoV-2 RBD has increased its human ACE2 (hACE2) binding affinity compared with that of SARS-CoV [15],[16]. The transmembrane S2 domain contains heptad repeat regions and the fusion peptide, which mediate the fusion of viral and cellular membranes upon extensive conformational rearrangements [10] (Fig 2).

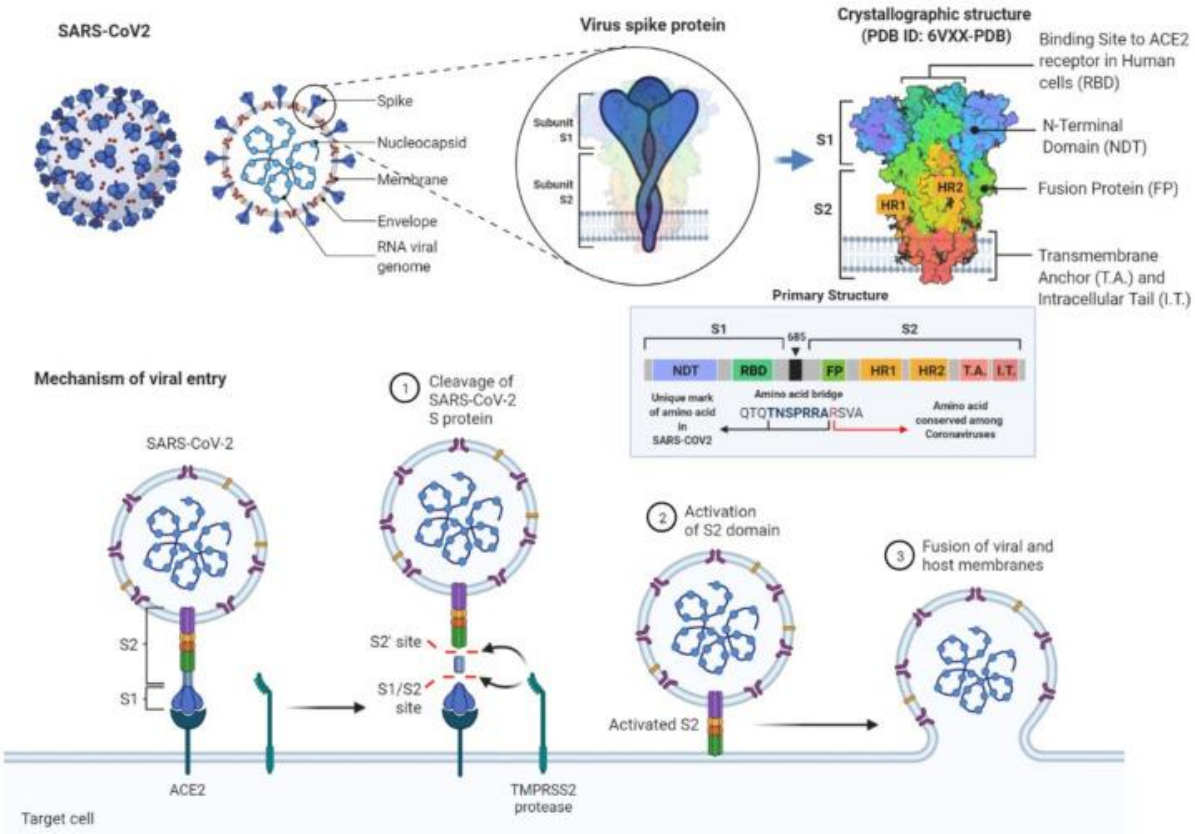

Figure 2. The schematic representation of the SARS-CoV-2 and its surface spike protein structure with their structural descriptions and detailed mechanisms of the viral entry to cells during infection. Spike protein plays a crucial role in this process. While S1 subunit is responsible for anchoring the virion by binding to the cellular receptor angiotensin-converting enzyme 2 (ACE2) of the host cell, S2 subunit enhances the fusion of the viral and the host cell membranes. The fusion is mediated by the S2 subunit that is activated by the transmembrane protease serine 2 (TMPRSS2)

cleaving the spike protein at the S1/S2 sites. From Petrovszki, Dániel et al. “Penetration of the SARS-CoV-2 Spike Protein across the Blood-Brain Barrier, as Revealed by a Combination of a Human Cell Culture Model System and Optical Biosensing.” Biomedicines vol. 10,1 188. 17 Jan. 2022, doi:10.3390/biomedicines10010188.

A distinctive feature of the SARS-CoV-2 S protein is the acquisition of a polybasic cleavage site (PRRAR) at the S1–S2 junction, which permits efficient cleavage by the prototype proprotein convertase furin. A study suggested that the furin-cleavage site can reduce the stability of SARS-CoV-2 S protein and facilitate the conformational adaption that is required for the binding of the RBD to its receptor [17]. Similarly to other coronaviruses, SARS-CoV-2 needs proteolytic processing of the S protein to activate the endocytic route. It has been shown that host proteases participate in the cleavage of the S protein and activate the entry of SARS-CoV-2, including transmembrane protease serine protease 2 (TMPRSS2), cathepsin L and furin. The spike protein is mainly cleaved by furin, present on the host cell surface membrane, into the S1 and S2 components corresponding to the prefusion state. The subsequent fusion is considered to involve a second cleavage by a serine protease or by endosomal cysteine proteases, triggering S1 dissociation and irreversible S2 folding into a fusion state conformation [18],[19],[20]. TMPRSS2 is highly expressed in several tissues and body sites and is co-expressed with ACE2 in nasal epithelial cells, lungs and bronchial branches, which explains some of the tissue tropism of SARS-CoV-2 [10],[21]. Cleavage results in enhanced infection and has been proposed to be a key factor in SARS-CoV-2 evolution. An efficient S protein cleavage is required for successful infection and is a main determinant in overcoming species barriers [10]. These major structural rearrangements in S protein are required for cell and viral membrane fusion and for the viral RNA release into the cytoplasm[3], [5],[19].

Therefore, the S glycoprotein is crucial for the entry of SARS-CoV-2 and represents an excellent target for anti-viral therapeutic development [22].

Angiotensin converting enzyme (ACE2) receptor

Several coronavirus receptors have been identified and include human aminopeptidase N (APN; HCoV-229E), angiotensin-converting enzyme 2 (ACE2; HCoV-NL63, SARS-CoV and SARS-CoV-2) and dipeptidyl peptidase 4 (DPP4; MERS-CoV). ACE2 was identified as the functional receptor that enables infection by SARS-CoV. The high genomic and structural homology between the S proteins of SARS-CoV and SARS-CoV-2 sustained the identification of ACE2 as the cell-surface receptor for SARS-CoV-2. Furthermore, human ACE2, SARS-CoV-2 also recognizes ACE2 from pig, ferret, rhesus monkey, civet, cat, pangolin, rabbit and dog [8]. ACE2 is widely expressed in human, including lung alveolar epithelial cells, small intestinal epithelial cells, cardiovascular system, central nervous system, and kidney. The expression and tissue distribution of receptors influence viral tropism and pathogenicity [10],[21],[23]. ACE2 plays a counterbalance action in the renin-angiotensin-aldosterone system (RAAS), catalyzing with high efficiency the conversion of the AngiotensinII (Ang) II in Ang1-7, which is a critical regulator of blood volume and systemic vascular resistance and contributes to sodium reabsorption, inflammation, and fibrosis, preventing the possible adverse effect of AngII accumulation [24]. There are two forms of ACE2. The full-length mACE2 is located on cell membranes and consists of a transmembrane anchor and an extracellular domain (sACE2). The second form, sACE2, is a soluble form that is shed into the circulation. This form of ACE lacks membrane anchors and circulates in low concentrations. The expression level of ACE2 and the ratio between mACE2 and sACE2 could explain why some people experience more severe

symptoms than others [24]. Unexpectedly, the analysis of ACE2 expression in experimental models and in human transcriptome revealed that it is very low in the lung, mainly limited to a small fraction of type II alveolar epithelial cells. Since most infected people present respiratory difficulties in response to SARS-CoV-2 infection, these findings were explained by the fact that the release of inflammatory cytokines, such as interferons (IFNs) caused by SARS-CoV-2, can increase the ACE2 expression and potentiate the infection. On the other side, the ACE2 shedding can be stimulated by proinflammatory cytokines such as IL-1β and tumor necrosis factor (TNF)-α, and endotoxin that could result in a reduction of SARS-CoV-2 entry, but at the same time, may cause an increase in AngII and further activation of the AngII/AT1R axis increasing inflammation [24]. It is surprising that SARS-CoV and SARS-CoV-2 display differences in virus replication efficiency and spread. SARS-CoV targets pneumocytes and lung macrophages in lower respiratory tract tissues, where ACE2 is predominantly expressed, consistent with the lower respiratory tract disease resulting from SARS-CoV infection and the limited viral spread. By contrast, SARS-CoV-2 replicates both upper, abundantly and where ACE2 is also located, and lower respiratory tract tissues and is efficiently transmitted human-to-human even before the onset of symptoms [10].

COVID-19: Pathogenesis and Treatment Approaches

SARS-CoV-2-infected patients start experiencing flu symptoms like fever, cough, nasal congestion. As the viral infection progresses, patients often experience dyspnea and consistent symptoms of viral pneumonitis, such as decreased oxygen saturation, lymphopenia, and alveolar exudates with intralobular involvement in chest imaging. Therefore, the outcome of these patients is a severe condition of acute lung injury, named acute respiratory distress syndrome (ARDS). ARDS is characterized by

respiratory distress associated with hypoxemia and the presence of bilateral infiltrate on chest imaging [25]. The pathogenesis of SARS-CoV-2 infection is characterized by mild symptoms to severe respiratory failure. On binding to epithelial cells in the respiratory tract, SARS-CoV-2 starts replicating and migrating down to the airways and enters alveolar epithelial cells in the lungs. The rapid replication of SARS-CoV-2 in the lungs may trigger a strong immune response. Cytokine storm syndrome causes acute respiratory distress syndrome and respiratory failure, which is considered the main cause of death in patients with COVID-19. Patients with serious pre-existing diseases have a greater risk of developing ARDS and death. Multiple organ failure has also been reported in COVID-19 cases [8] (Fig. 3). During the virus replication, the host's immune system is activated, inducing the recruitment of inflammatory cells with subsequent production of pro-inflammatory cytokines and chemokines, as well as maturation of dendritic cells. However, due to the continuous and rapid viral genome replication, the immune system is continuously activated, culminating in an uncontrolled and exacerbated response, lethal to host cells. Monocytes recruited into the alveolar space secretes proinflammatory cytokines and induces pneumocytes apoptosis through the release of IFN dependent on Alpha TNF-α, activating cell death receptors. In addition, recruited macrophages releases chemokines and other cytokines responsible for increasing capillary permeability and consequent neutrophils recruitment. The excessive neutrophil degranulation causes permanent damage into pneumocytes and endothelial cells, breaking alveolar-capillary barrier [25]. Consequent to this was observed tissue edema, endotheliitis, and disseminated intravascular coagulation (DIC) pathways with inflammation in multiple organs (lung, heart, kidney, small bowel, and liver) in patients with severe COVID-19 (Fig. 3) [14].

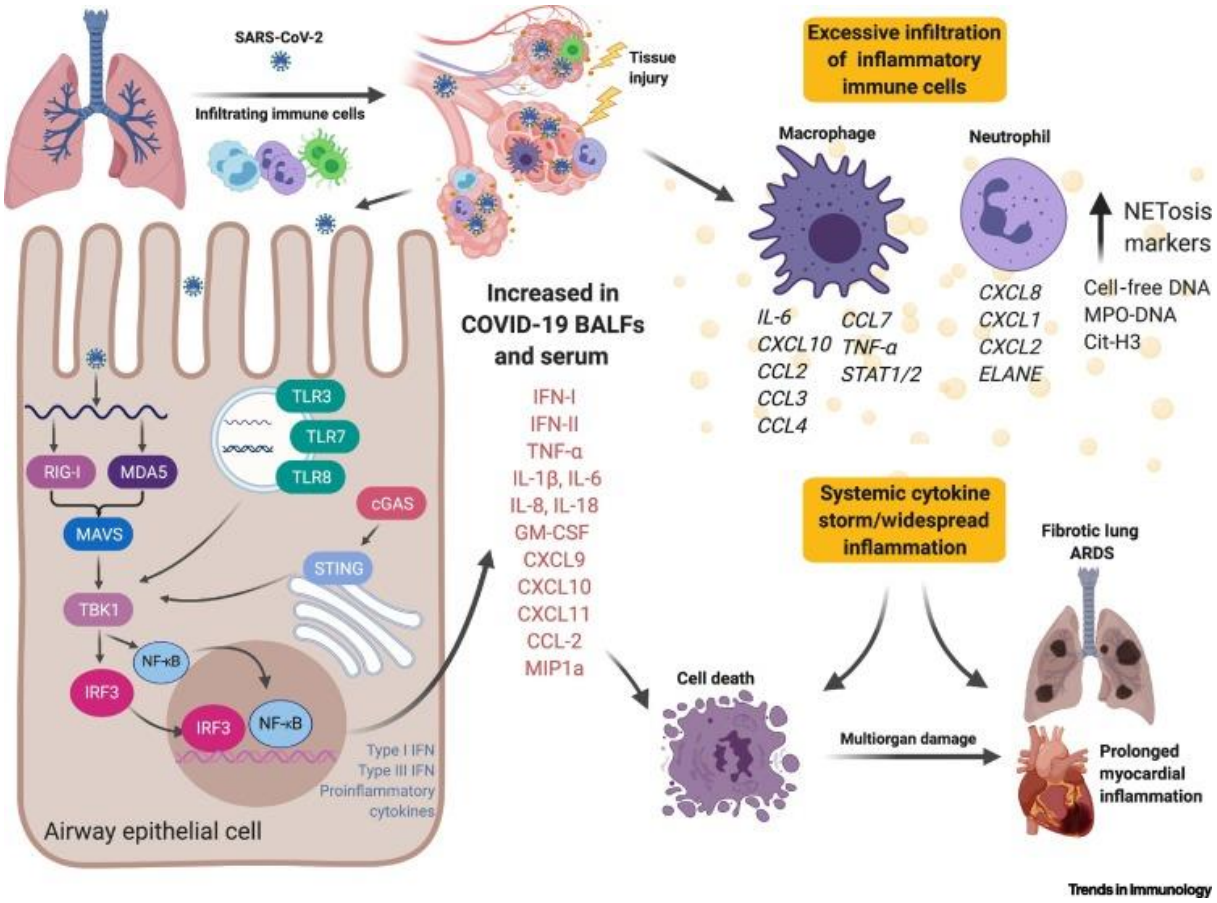

Figure 3. **Following inhalation of severe acute respiratory syndrome coronavirus 2 (SARS-CoV-2) into the respiratory tract, the virus traverses deep into the lower lung, where it infects a range of cells, including alveolar airway epithelial cells, vascular endothelial cells, and alveolar macrophages.** Upon entry, SARS-CoV-2 is likely detected by cytosolic innate immune sensors, as well as endosomal toll-like receptors (TLRs) that signal downstream to produce type-I/III interferons (IFNs) and proinflammatory mediators. The high concentration of inflammatory cytokines/chemokines amplifies the destructive tissue damage via endothelial dysfunction and vasodilation, allowing the recruitment of immune cells, in this case, macrophages and neutrophils. Vascular leakage and compromised barrier function promote endotheliitis and lung edema, limiting gas exchange that then facilitates a hypoxic environment, leading to respiratory/organ failure. The inflammatory milieu induces endothelial cells to upregulate leukocyte adhesion molecules, thereby promoting the accumulation of immune cells that may also contribute to the rapid progression of respiratory failure. Hyperinflammation in the lung further induces transcriptional changes in macrophages and neutrophils that perpetuate tissue damage that ultimately leads to irreversible lung damage. Recent evidence suggests that systemic inflammation induces long-term sequela in heart tissues. Abbreviations: BALF, bronchoalveolar lavage fluid; IRF3, interferon regulatory factor 3; NF-κB, nuclear factor-κB; RIG-I, retinoic acid-inducible gene I; STAT1/2, signal transducer and activator of transcription 1/2; STING, Stimulator of interferon genes. Figure from Harrison, Andrew G et al. “Mechanisms of SARS-CoV-2 Transmission and Pathogenesis.” Trends in immunology vol. 41,12 (2020): 1100-1115. doi:10.1016/j.it.2020.10.004.

The various COVID-19 treatments can be classified into two major categories based on their targets: antiviral agents and therapies that target the host. Antiviral agents identified to contrast COVID-19 primarily include polymerase inhibitors, protease inhibitors, nucleoside and nucleotide reverse transcriptase inhibitors, as well as entry

and uncoating inhibitors, combined with other antiviral medications. Therapies focused on the host include neutralizing antibody therapy, Janus kinase inhibitors, and steroids. Actually, the therapies are able to target symptoms caused by infection, but additional efforts are still required to advance the development of effective treatments for COVID-19 [26] (Fig. 4).

In the absence of specific antiviral therapies for SARS-CoV-2 infection and its associated pathology, the pivotal solution remains the prevention of infection through vaccination. The current challenge in the development of vaccines remains in achieving long-term efficacy in blocking SARS-CoV-2 infection. The World Health Organization (WHO) is at present maintaining publicly accessible the list of all the vaccines under clinical or preclinical evaluation (https://www.who.int/publications/m/item/draft-landscape-of-covid-19-candidate-vaccines). Actually, 183 is the number of vaccines in clinical development and 199 the number of vaccines in pre-clinical development [27].

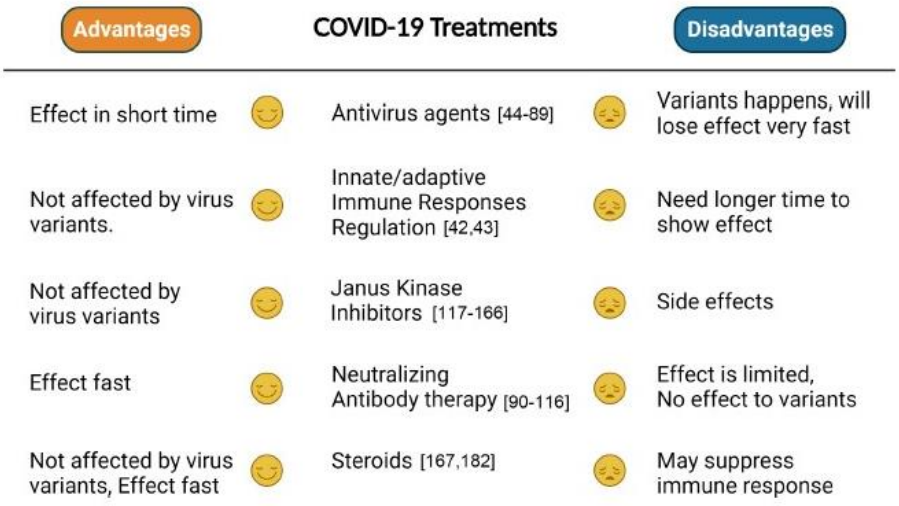

Figure 4. Comparison between different COVID-19 treatments. The advantages and disadvantages of each treatment are summarized on the basis of whether they will be efficient to variants, have side effects, or effect fast. Figure from Yuan, Yongliang et al. "The development of COVID-19 treatment." Frontiers in immunology vol. 14 1125246. 26 Jan. 2023, doi:10.3389/fimmu.2023.1125246.

Extracellular Vesicles and COVID-19

Extracellular Vesicles (EVs)

Extracellular Vesicles (EVs), a various group of membrane-bound vesicles, play a central role as vector for cell-to-cell communication through the release of bioactive factors (proteins, lipids and genetic material) and are involved in physiological and pathological processes. Their complex cargo reflects the type and pathophysiological status of the originating cell and so represents an important source of information [28],[29]. They are released by a wide range of cell types and can be categorized into two main types based on their origin: exosomes, released from the endosomal compartment with an average size of 100 nm, and ectosomes, released through budding of the plasma membrane, ranging in size from microvesicles to larger vesicles (50 nm to 1 µm). Other types of EVs include apoptotic bodies released by cells undergoing apoptosis, large tumor-derived vesicles (oncosomes), and vesicles derived from mitochondria (mitovesicles) [30].

The progressive inward folding of the plasma membrane results in the formation of early endosomes, which harbor cell-surface proteins and extracellular components. The maturation process of endosomes involves the generation of late-sorting endosomes, subsequently forming intracellular multivesicular bodies that harbor intra-luminal vesicles, predecessors to exosomes. The sorting and content determination of endosomes are orchestrated by the trans-Golgi network and the endoplasmic reticulum. Multivesicular bodies have the option to either fuse with lysosomes for degradation or with the cellular membrane to liberate mature exosomes (extracellular vesicles) into the extracellular space. Microvesicles, originating from the shedding of the plasma membrane, encompass cell-surface proteins and cytoplasmic components

(Fig. 5). Once released, both extracellular vesicles and microvesicles can be internalized by target cells releasing their contents. Additionally, they have the capacity to activate target cells through ligand binding to cell-surface receptors [29],[30]. Variations in size and surface molecules can influence the internalization ability of EVs. Multiple mechanisms of EV entrance in target cells have been identified, encompassing endocytosis, micropinocytosis, phagocytosis, plasma or endosomal membrane fusion, and endocytosis mediated by clathrin or caveolin. Upon cellular uptake, EVs may release their entire cargo into the cytoplasm. This transfer of biological material, including extracellular RNAs, small non-coding RNA species, lipids, and proteins, has the potential to modify recipient cells. Once internalized, the EVs can undergo degradation by lysosomes or be recycled and released back into the extracellular space. Moreover, EVs can activate target cells through receptor–ligand interactions without necessarily being internalized and delivering their contents [30]. Due to the transfer of bioactive molecules cargo and that EVs can be isolated from all biofluids, studies of EV cell biology are not only important to reveal new cell biological pathways but are also critical to open new possibilities for clinical use of EVs as disease biomarker. EVs are naturally taken up by target cells and can be used for transferring therapeutic agents and are therefore being considered as attractive candidates for potential therapeutic tools. The EV engineering has been considered helpful to increase the EV capabilities and to realize efficient drug delivery systems [31].

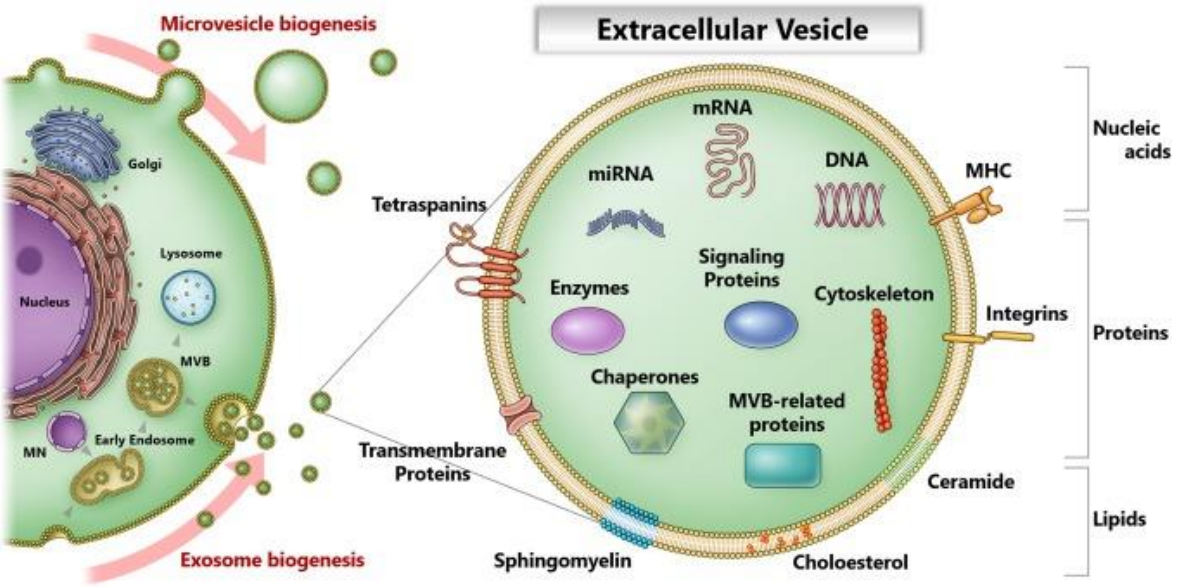

Figure 5. Extracellular vesicle biogenesis and components. A. Microvesicle (MV) biogenesis comprises several steps, including plasma membrane reorganization, redistribution of phospholipids, outward repositioning of phosphatidylserine, disassembly of the cytoskeleton network, and actomyosin basal abscission. B. Exosome biogenesis starts inward of the plasma membrane to form early endosomes. Intraluminal vesicles (ILVs) are formed, and the endosomes mature to multivesicular bodies (MVBs). MVBs fuse with the plasma membrane to release ILVs into the extracellular space, where they are then referred to as exosomes. Alternatively, the MVBs can fuse with lysosomes, resulting in the degradation of ILVs. C. EVs can contain nucleic acids (DNA and/or RNA), membrane anchored-proteins, cytosolic proteins, and lipids; these contents can vary depending on the releasing cell types and their conditions. Figure from Yokoi, Akira, and Takahiro Ochiya. "Exosomes and extracellular vesicles: Rethinking the essential values in cancer biology." Seminars in cancer biology vol. 74 (2021): 79-91. doi: 10.1016/j.semcancer.2021.03.032.

Viruses and EVs

It is already known that EVs and viruses share common aspects: size, structure, biogenesis, uptake, and the ability to carry a specific cargo while being different entities [32],[33]. Although some EVs can be up to 1μm in size, most are less than 300 nm in diameter, which is the size of a typical RNA virus [6]. Just as most coated viruses, with an outer phospholipid bilayer called the pericapsid or envelope, EVs are also surrounded by a phospholipid bilayer that also contains cell membrane proteins. Like many viruses, EVs are formed in the endosomal system or on the plasma membrane through defined biogenesis pathways involving, for example, the endosomal sorting complexes required for transport (ESCRT) machinery [34]. Recent findings demonstrate that viruses take advantage of EVs for cellular release, and EVs control

viral entry mechanisms for cargo delivery [32]. The viruses use EV endocytic routes to enter uninfected cells and change the EV secretory pathway to exit infected cells, thus illustrating that EVs and viruses share common cell entry and biogenesis mechanisms [32]. Like viruses, EVs can bind to plasma membranes of other cells, enter them through membrane fusion or by endocytosis, triggering specific reactions by recipient cells that may be cargo-dependent [34],[35]. Furthermore, exosomes from infected cells can contain viral components, which are important mediators of antiviral responses which make them ideal for a new vaccine, as well as vehicles that facilitate the spread of viral infection [33]. Interesting, EVs generated by infected cells with viral origin material and may be so similar to noninfectious defective viruses, that have lost the ability to replicate, that to discriminate the difference between the two is not easy [36]. In other cases, EVs provide an "envelope" for viruses without an envelope, e.g., in hepatitis A, the virus can be encapsulated in EVs and can infect cells by taking advantage of transport by EVs [37]. Similarly, EVs released from cells infected with hepatitis C can carry entire viral genomes that, in target cells, can generate new infectious viral particles [38]. In addition, exosomes contain receptors for viruses that make recipient cells susceptible to virus entry [39].

Studies indicated a significant increase in the secretion of EVs from cells infected with SARS-CoV-2, demonstrating that they play an important role in the pathogenesis of disease EVs may contribute to the infection, internalization and transmission of SARS-CoV-2 virus [40]. Recently, it was demonstrated that EVs from plasma patients with COVDI-19 are enriched in cardiovascular, inflammatory and procoagulant proteins according to the severity of disease [41], [42].

EVs may contribute to the spread of SARS-CoV-2 because they can transfer receptors such as ACE2 that makes cells responsive to the virus. Upon entry, SARS-CoV-2 virus

can be directed to the exosomal pathway, and its genetic component is packaged into exosomes [39] (Fig. 6).

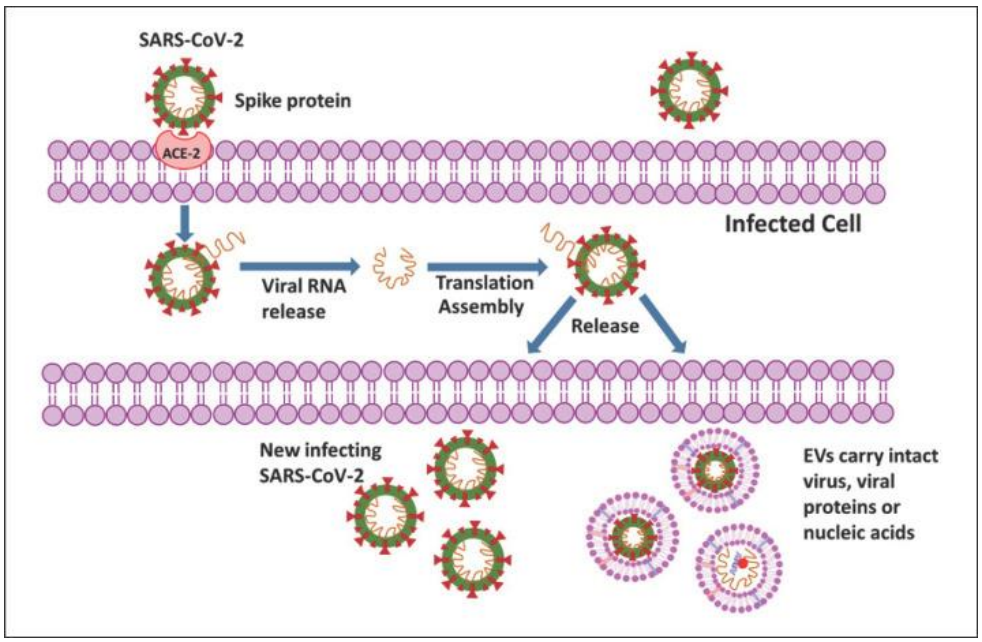

Figure 6. Schematics of SARS-CoV-2 viral replication in host cells. Figure from Pocsfalvi, Gabriella et al. "COVID-19 and Extracellular Vesicles: An Intriguing Interplay." Kidney & blood pressure research vol. 45,5 (2020): 661-670. doi:10.1159/000511402.

EV-based Therapies for COVID-19

There is an increasing number of clinical investigations to find therapeutic solutions to the various forms of the COVID-19 disease. The acute lung injury is the most severe impact of COVID-19. Host response promotes the damage in pulmonary tissue, reduction in total function and reduced lung capacity depending on lack of control over immune response [43]. Studies focused on the regeneration of damaged cells as well as on the blocking or modulating of inflammatory responses [7], [32]. Mesenchymal stromal cell- EVs (MSC-EVs) are being intensively under investigation for the treatment of COVID-19 [32]. MSC-derived EVs are studied in various aspects of COVID19, including their use as biomarkers for diagnostic purpose, or, when engineered, as

immune-modulating agents, targeted therapeutic cargo, as well as vaccines. MSC-EVs in pre-clinical models of pulmonary diseases showed the most common effect in an improvement in the lung function [44]. The potential of MSC-EVs in repairing and regenerating tissue is of great interest considering the lesions reported after SARS-CoV-2 infection. It was described that MSC-EVs stimulated the repopulation of type II alveolar cells which serve as a progenitor cell for lung epithelium [45].There is a growing interest in the new potential application of EV as a disease treatment strategy. In particular, the engineering of EVs could be attractive for anti-viral purposes. Recent studies demonstrated that ACE2-engineered EVs limit the SARS-CoV-2 infection [46],[47]. Another work demonstrated the possibility of using EVs modified with the only receptor-binding domain (RBD) of the viral spike protein, that recognizes ACE2 receptor, as a target delivery system of potential anti-viral agents *in vivo* [48],[49].

The use of EVs as immunogenicity factors in the treatment of SARS-CoV infection has been studied. After evaluating it to an adenoviral vector vaccine expressing the S protein, it has been proved that both exosomes and the vaccine could induce neutralizing antibody titers. Furthermore, the treatment of EVs has been shown to be more effective than soluble protein subunit vaccines, because EVs can express multiple copies of the same viral protein and promote the cross-linking between EVs and the B cell receptor [50].

Interestingly, exosomes enriched in ACE2 protein were developed to induce a competitive inhibition- mediated binding of the exosomes to the SARS-CoV-2 virus. One study used bone marrow-MSC expressing in stable way the ACE2 receptor and the exosomes were isolated from them (patent no. CN112430581A). One more patent suggests the possibility to use vesicles expressing a chimeric ACE2 receptor to delivery Remdesivir on the coronavirus binding site (patent no. CN112522203A).

Alternatively, Scott et al propose a molecular therapy aimed at neutralizing SARS-CoV-2, via EVs containing a fusion protein, specifically a CD63 tetraspanin bound to an anti-CoV-2 nano-antibody. These EVs obtained from HEK293 enriched with an anti-CoV-2 Ab bind the S protein S of SARS-CoV-2 at the level of the RBD and can functionally neutralize SARS-CoV-2 [51]. A report suggested a plasmid constructed with spike-lamp2b and transfected in mouse dendritic cells. The exosomes secreted by these cells carried spike protein and were able to induce antibody synthesis after human injection (Patent No. CN112111513A).

Colchicine: an old drug and new use

Colchicine is an immunomodulatory old drug with new potential applications. It is extracted from the plant Colchicum autumnale and is widely used for its anti-inflammatory effects [52], [53]. The anti-inflammatory capabilities of colchicine depend on its antagonism in microtubule polymerization due to its strong ability to bind tubulin by disturbing the dynamic assembly of microtubules [54]. It is commonly used in various pathologies such as gout, familial mediterranean fever and rheumatoid arthritis, and non-rheumatic diseases such as pericarditis and atherosclerosis [52], [55], [56] . Consequently, to its microtubule antagonism, colchicine interferes with several inflammatory pathways, including inhibition of neutrophil chemotaxis, adhesion, and mobilization; disruption of superoxide production, inflammasome inhibition, and tumor necrosis factor reduction; and its possible antiviral properties [57]. Furthermore, colchicine was tested as a clinical trial for COVID-19 treatment with promising results [58],[59]. Several studies have proposed the use of colchicine for chronic hepatitis, post-hepatic cirrhosis, biliary cirrhosis, and alcoholic cirrhosis. Recently, colchicine has been shown to be effective in patients with post-transplant

capillary leak syndrome and renal failure [60]. Additionally, microtubules are considered an ideal target for anticancer drugs because of their essential role in mitosis [61], therefore various studies suggested the use of colchicine also for cancer therapy [54],[56],[61],[62]. Colchicine represents a huge economic and health advantage by being a widely available, safe, and low-cost drug. However, the mechanisms of action of colchicine are not entirely clear. Further investigations are essential for the development of therapeutic protocols for the use of colchicine to prevent/contrast pathologies such as virus infections and cancer progression, reducing the economic, health, and death impact worldwide.

Aim of the work

The aim of this work was to generate a simple, safe, and scalable model to study therapeutic approaches against SARS-CoV-2 infection, such as block of the cell binding and of virus internalization, through the analysis of EV properties. For this purpose, we generated EVs expressing spike protein (S-EVs) and characterized them using western blot, MACSPlex, ExoVieW and super resolution microscopy.

The EV-cell interaction was analyzed using supported lipid bilayer, cell membrane model, in which we assessed the possible fusogenic effect of spike protein. Moreover, we evaluated the S-EV uptake capability between ACE2 positive and negative cells in order to validate the specificity of S-ACE2 receptor interaction.

Finally, to test new therapeutic approaches, we studied the effect on S-EV uptake of anti-ACE2 blocking antibody or colchicine, a microtubule antagonist and anti-inflammatory drug. To further explore the potential role of colchicine in the EV uptake inhibition, we isolated and characterized EVs from tumor cells (SKOV3 and HT29 cells) and we assessed the tumor-EV entrance in physiological (HMEC) and in endothelial cancer (EcK) cells after colchicine treatment.

Materials and Methods

Cell Cultures

Human embryonic kidney cells (HEK293T) SARS-CoV-2-spike-transfected (H-S) or not transfected (H-C) cell lines were purchased from LiStarFish (Milan, Italy) and cultured in the high glucose Dulbecco's Modified Eagle Medium (DMEM) (Thermo Fisher Scientific, Waltham, MA, USA) adding 10% of fetal bovine serum (FBS) (Euroclone, Milan, Italy) and with 100 U/mL of penicillin/streptomycin. The H-S were transfected with mammalian expression vector, the pCMV3-2019-nCoV-spike (S1+S2)-long plasmid. The transfection quality control was confirmed by full-length sequencing using the primers pCMV3-F: 5' CAGGTGTCCACTCCCAGGTCCAAG 3', pcDNA3-R: 5' GGCAACTAGAAGGCACAGTCGAGG 3' or T7-F: 5' TAATACGACTCACTATAGGG 3', BGH-R: 5' TAGAAGGCACAGTCGAGG 3') and validated by the expression of SARS-CoV-2 spike protein in cells surface membrane. Hygromycin (80 g/mL) was added to the H-S medium during every 3 passages to select the transfected cells. The immortalized normal human bronchial epithelial (16HBE14o-) cell line was kindly provided by Dr. Alessandra Ghigo (University of Turin, Italy) who originally received the cells from Dr. Dieter Gruenert (University of California San Francisco, San Francisco, CA, USA). 16HBE14o- were cultured in Minimum Essential Medium (MEM) (Lonza, Basel, Switzerland) supplemented with 10% of FBS (Euroclone, Milan, Italy) and 100 U/mL of penicillin/streptomycin on culture dishes pre-coated with human fibronectin (1 mg/mL; Sigma-Aldrich, Saint Louis, MO, USA), bovine collagen I (3 mg/mL; Sigma-Aldrich, Saint Louis, MO, USA) and bovine serum albumin (0.1%). Primary human umbilical vein endothelial cells (HUVEC) and human microvascular endothelial cell line (HMEC) were purchased from ATCC (ATCC-PCS-100-010, Manassas, VA, USA), the human renal endothelial cancer cells were (EcK)

isolated from renal cell carcinoma by B. Bussolati et al. in 2003 [63]. The endothelial cells were cultured in the EndoGRO VEGF Supplement Kit (Millipore Sigma™, Burlington, MA, USA) adding 5% FBS according to the protocol observed in previous studies [64],[65]. Human lung fibroblast cells (MRC5), human proximal tubular cells (HK-2) and human colorectal cancer cells (HT29) were purchased from Sigma-Aldrich (St. Louis, MO, USA) and were cultured in DMEM low glucose in the presence of 10% FBS and 100 U/mL of penicillin/streptomycin [66],[67]. The renal cancer stem cells (G7) were isolated characterized by Dr. Alessia Brossa and colleagues [68]. G7 were obtained from specimens of renal cell carcinomas from patients undergoing radical nephrectomy according to the Ethics Committee of the S. Giovanni Battista Hospital of Torino, Italy (168/2014). G7 were isolated from the total RCC population, using anti-CD105 Ab by magnetic-activated cell sorting (MACS) system (Miltenyi Biotec, Auburn, CA) and cultured in the presence of the expansion medium, consisting of DMEM low glucose (Invitrogen, Carlsbad, CA), with insulin–transferrin–selenium, 10−9 M dexamethasone, 100 U penicillin, 1,000 U streptomycin, 10 ng/ml EGF (all from Sigma-Aldrich, St. Louis, MO) and 5% FBS [68]. Ovarian cancer cell line (SKOV3) was purchased from ATCC (ATCC-PCS-100-010, Manassas, VA, USA) and cultured in RPMI-1640 medium (Euroclone, Milan, Italy) and 10% FBS and 100 U/mL of penicillin/streptomycin [69]. The cell culture incubation was performed in incubator at 37 ºC with 5% CO2 and controlled humidity.

EV Isolation and Characterization

The S-EVs, C-EVs, SKOV3-EVs and HT29-EVs were obtained from supernatants of H-S, H-C, SKOV3 or HT29 cells respectively, cultured 16 h in RPMI deprived of FBS. After removal of cell debris and apoptotic bodies by centrifugation at 3000 g for 20 min,

EVs were purified by 2 h ultracentrifugation at 100,000 g at 4 ºC (Beckman Coulter Optima L-90 K; Fullerton, CA, USA). EVs were used fresh or stored at -80 ºC after resuspension in RPMI supplemented with 1% dimethyl sulfoxide (DMSO). Analysis of size distribution and enumeration of EVs were performed using nanoparticle tracking analysis NS300 (Malvern Instruments Ltd, Malvern, UK) equipped with a 488nm laser and the nanoparticle tracking analysis 3.2 software.

ExoView Analysis

Characterization of S-EVs markers was performed by using an ExoView Tetraspanins Kit (NanoView Bioscience, Boston, MA, USA). Each chip was coated with CD9, CD63, CD81 antibodies and MIgG control antibody. The chips were incubated with EV samples, using 35 µL of EV (1 x 10^9 particles/mL according to the nanoparticle tracking analysis) suspension, left overnight and protected from the light. After multiple washing steps, the chips were analyzed using ExoViewTM R100 imaging platform (NanoView, Bioscience, Boston, MA, USA) with ExoViewer software.

Super-Resolution Microscopy

Super-resolution microscopy analyses of S-EVs were performed using a temperature controlled Nanoimager S Mark II microscope from ONI (Oxford Nanoimaging, Oxford, UK) equipped with a 100x, 1.4NA oil immersion objective, an XYZ closed-loop piezo 736 stage, and 405 nm/150 mW, 473 nm/1 W, 560 nm/1 W, 640 nm/1 W lasers and dual/triple emission channels split at 640 and 555 nm. The samples were prepared using 10 L of 0.01% Poly-L-Lysine (Sigma-Aldrich, St. Louis, MO, USA) placed on cleaned high-precision coverslips and were placed at 37 C in a humid chamber for 2

h. After this time, excess Poly-L-Lysine was removed. A total of 1 µL of EVs (1 x10^{10}) resuspended in 9 µL of blocking solution (PBS-5%) was pipetted into a previously coated well to attach overnight at +4 ºC. The next day, the sample was removed, and 10 µL of blocking solution was added into the wells for 30 min. Then, 2.5 µg of purified mouse anti-CD9, anti-CD63, anti-CD81 (Oxford Nanoimaging, Oxford, UK), anti-SARS-CoV-2 S antibody (CRE-CABT-CS048B) or anti-SARS-CoV-2 S1(MAB105403) and anti-SARS-CoV-2 S2 (MAB10557) were conjugated with Alexa Fluor 555, 647, or 488 dyes using the Apex Antibody Labeling Kit (Invitrogen, Carlsbad, CA, USA), according to the manufacturer's protocol. The antibodies were left for overnight incubation at +4 C protected from the light. The samples were washed twice with PBS and a 10 µL ONI BCubed Imaging Buffer (Alfatest, Roma, Italy) was added for amplifying the EV fluorescence signal. Three-channel dSTORM data (2000 frames per channel) were acquired sequentially at 30Hz (Hertz) in the total reflection fluorescence (TIRF) mode. Single molecule data were filtered using NimOS (Version 1.18.3, ONI), based on the point spread function shape, photon count, and localization precision to minimize background noise and remove low-precision localizations. All pictures were analyzed by the CODI website platform www.alto.codi.bio (ONI). The filtering and drift correction was used as in NimOS software. The BDScan clustering tool was applied to merged channels, and EVs were counted co-localized or in separate channels.

Transmission Electron Microscopy

Transmission electron microscopy (TEM) was performed on S-EVs placed on 200-mesh nickel formvar carbon-coated grids (Electron Microscopy Science, Hatfield, PA, USA) and left to adhere for 20 min. The grids were then incubated with 2.5% glutaraldehyde containing 2% sucrose and, after washings in distilled water, the EVs

were negatively stained with NanoVan (Nanoprobes, Yaphank, NY, USA) and observed using a Jeol JEM 1010 electron microscope (Jeol, Tokyo, Japan).

MACSPlex Exosome Kit Analysis

C/S-EV, SKOV3-EV and HT29-EV samples were subjected to bead-based multiplex EV analysis by flow cytometry (MACSPlex Exosome Kit, human, Miltenyi Biotec, CA, USA), 1x 10^9 EV containing samples (concentration normalized using nanoparticle tracking analysis) were processed as follows: samples were diluted with MACSPlex Buffer (MPB) to a final volume of 120 µL. 15 µL of MACSPlex Exosome Capture Beads (containing 39 different antibodies-coated bead subsets) were added to each sample. Samples were then incubated on an orbital shaker overnight (14–16 h) at 450 rpm at +4 ºC, protected from light. To wash the beads, 1 mL of MPB was added and removed after several centrifugations (3000 g, 5 min). For counterstaining of EV bound by capture beads with detection antibodies, 135 µL of MPB and 5 µL of each APC-conjugated anti-CD9, anti-CD63, and anti-CD81 detection antibodies (provided in kit) or APC-conjugated SARS-CoV-2 spike S2 Subunit Antibody (MAB10557) and SARS-CoV-2 spike S1 Subunit Antibody (MAB105403) were added to each sample and were incubated on an orbital shaker at 450 rpm protected from light for 1 h at room temperature. After that, 1mL of MPB was added to wash the beads and then it was removed after one centrifugation (3000 g, 5 min). This step was followed by another washing with 200 µL of MPB, incubation on an orbital shaker at 450 rpm protected from light for 15 min at room temperature and then MPB was removed. Subsequently, 150 µL of MPB was added to each sample and flow cytometric analysis was performed.

EV Interaction with Supported Lipid Bilayer (SLB)

Small unilamellar vesicle preparation

The lipids, 1,2-dioleoyl-sn-glycero-3-phosphoCholine (18 : 1 (Δ9 $-Cis$) PC), Sphingomyelin (brain, porcine, SM), and cholesterol (ovine wool, > 98%), were purchased from Avanti Polar Lipids. The single lipids, suspended in chloroform, were mixed at the desired concentration and placed under vacuum overnight. The dry film was then hydrated with TRIS buffer (10 mM, pH 7.4), to obtain a final concentration of 1 mg/mL. The lipidic mixture was sonicated for 40 min at 45 ◦C and vortexed. Lastly, the resulting solution was extruded 51 times at 40 ◦C through a membrane with 100 nm pores (PC Membranes 0.1 µm, Avanti Polar Lipids) [70].

Supported lipid bilayer preparation

The supported lipid bilayer was composed by DOPC/SM (2:1 m/m) with cholesterol (10 mol%). The obtained extruded solution was diluted in TRIS/CaCl2 buffer to a final concentration of 0.4 mg/mL with 2 mM CaCl2. For the bilayer composition, the vesicle fusion method was adopted as a standard procedure for planar lipid bilayer preparation. The sample was deposited on a freshly cleaved mica substrate (Nano-Tec V-1 grade, 0.15 − 0.21 mm thickness, 10 mm diameter), incubated at 50 ◦C for 30 min, and slowly cooled to 27 ◦C, then extensively washed with TRIS buffer 10 mM [70].

Atomic force microscopy imaging

AFM was performed on commercially available microscope (Cypher ES from Asylum Research), working at 27 ◦C in high resolution AC mode. Sharp nitride levers (SNL −

10 with A geometry from Bruker Corporation) were used to perform the imaging in liquid conditions. Images were acquired at 512 × 512-pixel frames at 2.44 Hz [70].

Uptake of DiI-labeled EVs in Target Cells

In brief, 2.4 µL of vibrant™ DiI cell-labeling solution (Invitrogen, Carlsbad, CA, USA) was added to EV samples (C-EVs, S-EVs, SKOV3-EVs and HT29-EVs) and incubated for 20 min at 37 ºC. After the incubation, the labeled-EVs were purified with 1h ultracentrifugation at 100,000 g at +4°C and resuspended in RPMI +1% DMSO. A DiI control solution (CTL-DiI) was prepared using the protocol above, in the absence of EVs. HUVEC were incubated with 40,000 DiI-labeled EVs/target cells at 37 ºC for different time points (30 min, 1 h, or 3 h) to monitor EV internalization over time. In selected experiments, HUVEC were treated with anti-ACE2 blocking antibody at the concentration of 20 µg/mL (AF933, R&D Systems, Minneapolis, MN, USA) or colchicine 150 µM for 2 h. After the treatments, DiI-labeled-EVs were added to the medium for 3 h; at the end of experiments, cells were subjected to immunofluorescence analysis. Cells were extensively washed with PBS and fixed in paraformaldehyde (PAF) 4%. The FITC-phalloidin (Sigma-Aldrich, St. Louis, MO, USA) was used to label actin filaments of HUVEC and nuclei were stained with 4.6-diamidine-2-phenylindole (DAPI) (Sigma-Aldrich, St. Louis, MO, USA). Cells and EVs fluorescence were evaluated using an Apotome fluorescent microscope (Zeiss, Jena, Germany), magnification 40x.

Cytofluorimetric Analysis

HUVEC, 16HBE14o-, MRC5, H-S, H-C, G7, HK-2, HMEC and EcK were detached using a nonenzymatic cell dissociation solution and resuspended in PBS 0.1% BSA (Sigma-Aldrich, St. Louis, MO, USA) and incubated with antibodies according to the experimental protocols. The following antibodies conjugated conjugated with Alexa Fluor 488 and anti-S1 and anti S2 conjugated with Alexa Fluor 647 dyes using the Apex Antibody Labeling Kit, Invitrogen (Carlsbad, CA, USA) were used to characterize cells: ACE2 (AG-20A-0032TD) from Adipogen (Adipogen Life Sciences, CA, USA), spike (CRE-CABT-CS048B) from LiStarFish (Milan, Italy), S1 (MAB105403) and S2 (MAB10557) from R&DSystem (from Minneapolis, Minnesota, United States). Moreover, DiI-labeled-C/S-EV uptake by HUVEC and 16HBE14o- or DiI-labeled-SKOV3/HT29-EV uptake by HMEC or EcK were evaluated after 2h of colchicine/anti-ACE2 and 3 h of EVs, using cytofluorimetric analysis.

Western Blot

For protein analysis, the H-S and H-C and S/C-EVs were lysed at 4 ºC for 30 min in RIPA buffer (20 nM Tris HCl, 150 nM NaCl, 1% deoxycholate, 0.1% SDS 1% Triton X-100, pH7.8) supplemented with protease and phosphatase inhibitor cocktail and PMSF (Sigma-Aldrich, St. Louis, MO, USA). Total protein concentration was determined spectrophotometrically using a micro-BCA™ Protein Assay Kit, as previously described [71]. Proteins were separated by 4% to 20% gradient sodium dodecyl sulfate–polyacrylamide gel electrophoresis (SDS PAGE, Biorad, Milan, Italy) and subjected to immunoblotting using the following primary antibodies: rabbit polyclonal anti-S, anti-S1 and anti-S2, mouse monoclonal anti-CD63 (sc-5275, Santa Cruz

Biotechnology, Heidelberg, Germany) used as a positive control for EVs, anti-Calreticulin (#2891 Cell Signaling Technology, Milan, Italy) used as negative control for EVs and mouse monoclonal anti-GAPDH (sc-47724, Santa Cruz Biotechnology, Heidelberg, Germany) or actin (sc-47778, Santa Cruz Biotechnology, Heidelberg, Germany) were used as housekeeping for the cells. The protein bands were detected using rabbit or mouse peroxidase-labeled secondary antibody and visualized using an enhanced chemiluminescence detection kit and ChemiDoc™ XRS+ System (BioRad, Milan, Italy).

Statistical Analysis

Data are shown as mean ± SD. At least three independent replicates were performed for each experiment. Statistical analysis was carried out on Graph Pad Prism version 8.0.1 (GraphPad Software, Inc., San Diego, CA, USA) using the Paired t-test followed by ratio paired t-test and unpaired t-test followed by Mann Whitney test. Significance was set at probability value of $p < 0.05$.

Results

S-EV Generation and Characterization

We first validated the presence of spike on transfected cells by cytofluorimetric analysis (Fig. 7A). Cells were analyzed every 3 passages with comparable spike expression (data not shown). Transfection did not alter cell phenotype, as displayed by maintenance of the typical expression of CD146 and CD29 progenitor markers [72],[73] respect to the H-C (Fig. 7B). We demonstrated the expression of the full-length spike protein and of the lower molecular weight S2 subunit, after S1 cleavage, in the H-S by western blot (Fig. 7C). Afterwards, we isolated the S-EVs or C-EVs by 2 h ultracentrifugation at 100,000 g at +4 ºC. EVs were used fresh or stored at -80 ºC after resuspension in RPMI supplemented with 1% DMSO. The S-EVs were subjected to TEM analysis confirming their typical cup-shaped morphology and a size of about 100 nm (Fig. 7D). We did not observe any differences in S-EVs and C-EVs concentration and size distribution by the nanoparticle tracking analysis (Fig. 7E, F), obtaining homogenous population with a size between 50 to 200 nm (Fig. 7E, F). Western blot analysis confirmed the presence of the full-length spike, and in low amount of the S2 subunit, in the EVs obtained from H-S but not from H-C (Fig. 7G).

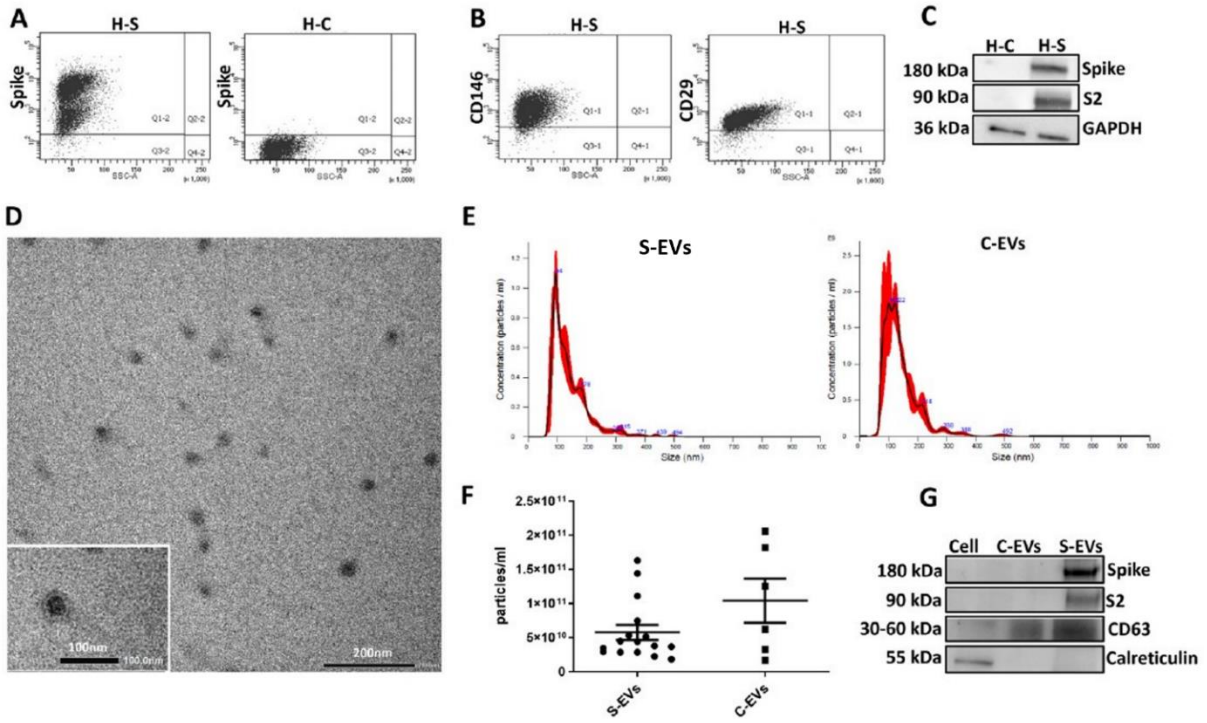

Figure 7. Characterization of H-S and EVs with validation of spike presence. (**A**) Representative flow cytometry analysis of spike protein in H-S and H-C. (**B**) Representative flow cytometry analysis of H-S showing positive expression of CD146 and CD29. (**C**) Representative western blot images of both full-length spike protein and S2 subunit (spike and S2) in H-S and H-C. GAPDH was used as an endogenous loading reference. (**D**) Representative micrograph of transmission electron microscopy of S-EVs (Scale bar: 200 nm; insert: 100 nm). (**E**) Representative nanoparticle tracking analysis of EVs from H-S cells (S-EVs) and from H-C cells (C-EVs) showing EV size distribution. (**F**) The graph shows EV sample quantifications. (**G**) Western blot images of spike subunits in S-EVs and C-EVs. CD63 was used as an exosomal marker and calreticulin as a negative EV marker. Figure from Verta, Roberta et al. "Generation of Spike-Extracellular Vesicles (S-EVs) as a Tool to Mimic SARS-CoV-2 Interaction with Host Cells." Cells vol. 11,1 146. 3 Jan. 2022, doi:10.3390/cells11010146.

Moreover, EVs were characterized by surface marker expressions, including tetraspanins, and typical markers of HEK293T cells, using a MACSPlex Exosome analysis kit after bead based immunocapture. The S-EVs resulted positive for all exosomal markers and for some progenitor cell surface markers as the control EVs, indicating that transfection did not alter surface marker expression (Fig. 8).

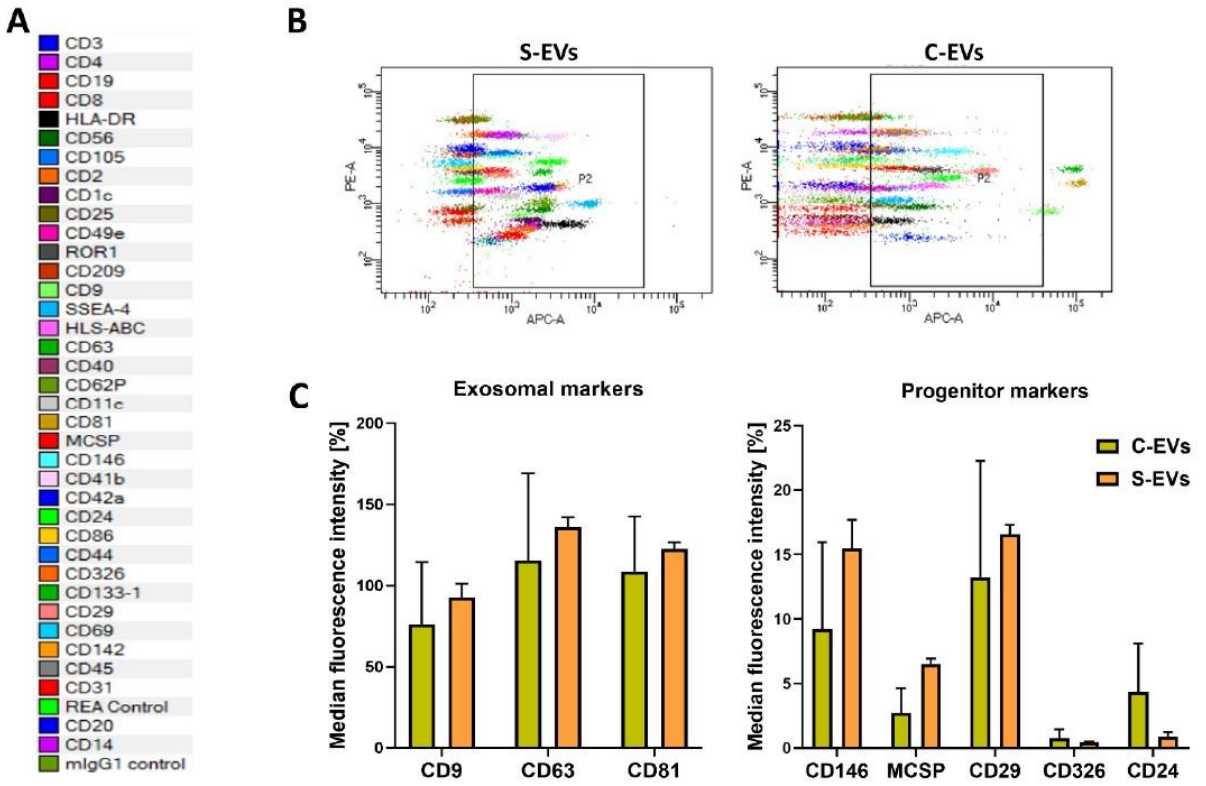

Figure 8. **Characterization of S-EVs.** (**A**) List showing the 39 antibodies used in the assay and their respective colors in dot plots. (**B**) MACSPlex representative dot plots showing the S-EVs and C-EVs distribution of allophycocyanin (APC)-stained bead populations. (**C**) Quantification of the median APC fluorescence for each bead population after background correction, clustered in exosomal and progenitor markers. The progenitor markers were normalized to median fluorescence intensity of exosomal markers. Data is expressed as the average of three independent experiments ± SD. Figure from Verta, Roberta et al. "Generation of Spike-Extracellular Vesicles (S-EVs) as a Tool to Mimic SARS-CoV-2 Interaction with Host Cells." Cells vol. 11,1 146. 3 Jan. 2022, doi:10.3390/cells11010146.

To better characterize spike-expressing EVs at a single EV level, EV size, morphology, and the co-localization of tetraspanins with spike protein were assessed using super-resolution microscopy and by ExoView chip-based analyses. Super-resolution microscopy confirmed spike expression by EVs, coupled with one, two or three tetraspanins CD9, CD63, and CD81 (Fig. 9). By CODI analysis, 19% of EVs were triple positive for the spike, CD63 and CD9 CD63 and CD9 and 13% of EVs were triple positive for the spike, CD81 and CD9 (Fig. 9A, B, C, D). The double positive on EV surface were 11% and 4% for spike with CD63 and spike with CD81 respectively (Fig. 9A, C). The spike and CD9 coexpression was between 6 and 11% (Fig. 9A, C). The percentage of EVs positive only for the spike was constant with 7% of expression (Fig.

9A, C). S-EVs represented between 35 and 43% of the total tetraspanin-expressing population (Fig. 9A, C). The super-resolution microscopy analysis confirmed the EVs size showed by nanoparticle tracking analysis and the mean size of EVs appeared as 100nm (Fig. 9B, D).

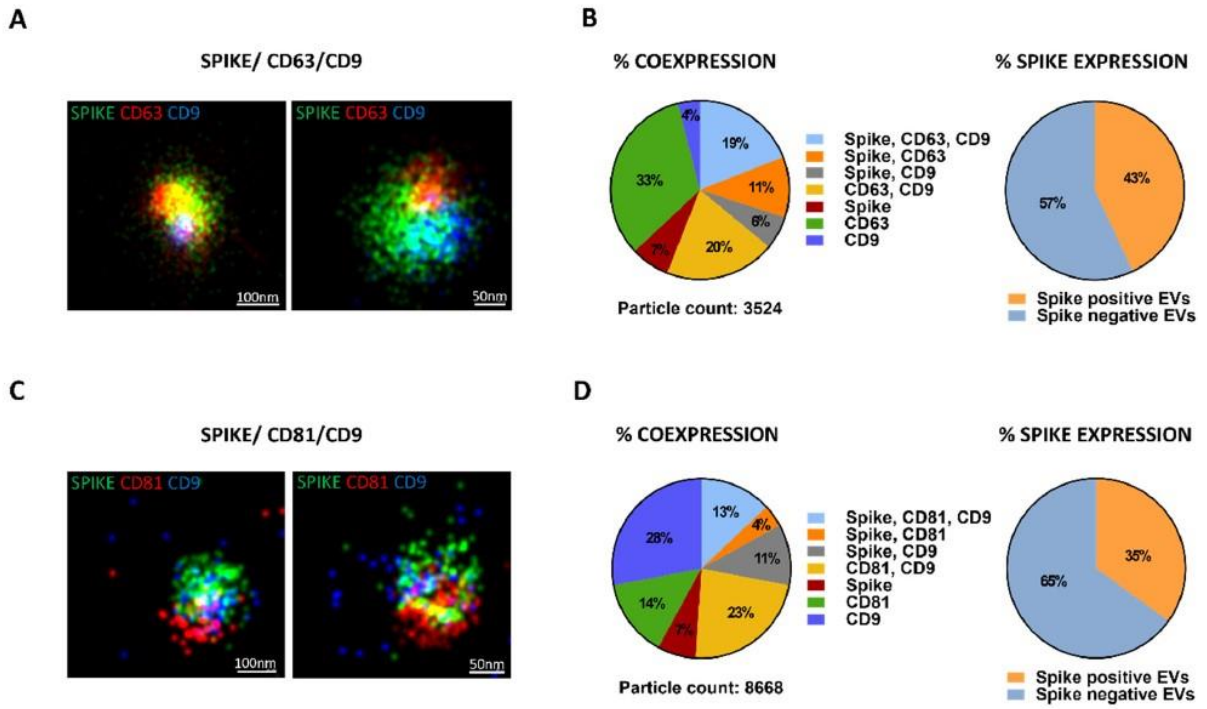

Figure 9. Super-resolution microscopy analysis of EVs isolated from H-S. (**A**) The percentage of EVs in triple, double or single positivity for spike, CD63, CD9 markers and the total percentage of EVs positive or negative for spike protein was reported. (**B**) Super-resolution microscopy micrographs showing the pattern distribution of spike in green, CD63 in red and CD9 in blue for S-EVs. (**C**) The percentage of EVs in triple, double or single positivity for spike, CD81, CD9 markers and the total percentage of EVs positive or negative for spike protein was reported. (**D**) Super-resolution microscopy micrographs showing the pattern distribution of spike in green, CD81 in red and CD9 in blue for S-EVs. Figure from Verta, Roberta et al. "Generation of Spike-Extracellular Vesicles (S-EVs) as a Tool to Mimic SARS-CoV-2 Interaction with Host Cells." Cells vol. 11,1 146. 3 Jan. 2022, doi:10.3390/cells11010146.

The spike co-expression with CD9, CD63 and CD81, on the EVs surface, was further confirmed using ExoView analysis, with similar expression levels on the single tetraspanin-affinity chips (Fig. 10 B).

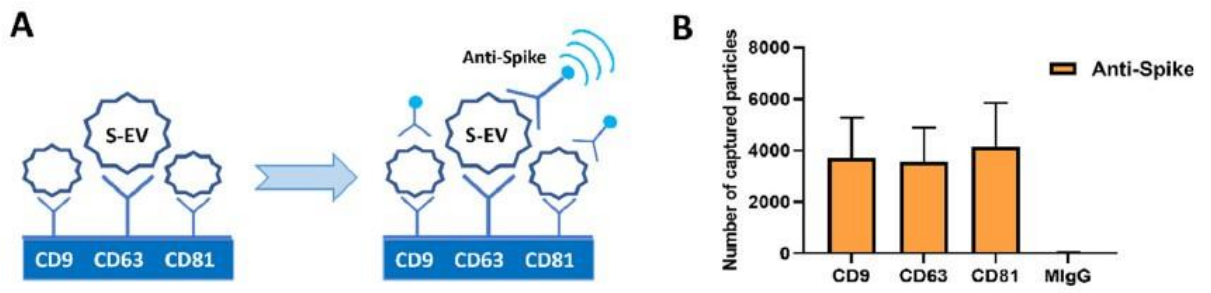

Figure 10. ExoView analysis of S-EVs. (**A**) Schematic representation of S-EVs detection process for ExoView technique. (**B**) Number of S-EVs captured on CD9, CD63, CD81 or MIgG spots fluorescently labeled by anti-spike ab in APC obtained by ExoView analysis. The graph shows the average of three independent experiments ± SD. Figure from Verta, Roberta et al. "Generation of Spike-Extracellular Vesicles (S-EVs) as a Tool to Mimic SARS-CoV-2 Interaction with Host Cells." Cells vol. 11,1 146. 3 Jan. 2022, doi:10.3390/cells11010146.

S1 and S2 presence on H-S

Due to the differential and functional activities of spike subunits for the SARS-CoV-2 virus infection, we characterize the spike for S1 and S2 subunit [74]. First, we demonstrated the S1 and S2 subunit presence by western blot from HEK293T-spike - transfected cells. The H-S express the trimeric spike protein (250-180 kDa), the S1 subunit (90 kDa) and the S2 subunit (75 KDa), in opposition to the H-C (Fig. 11). The presence of both subunits it was further demonstrated with cytofluorimetric analysis. The S1 and S2 positivity it was observed only in H-S but not in H-C (Fig. 11).

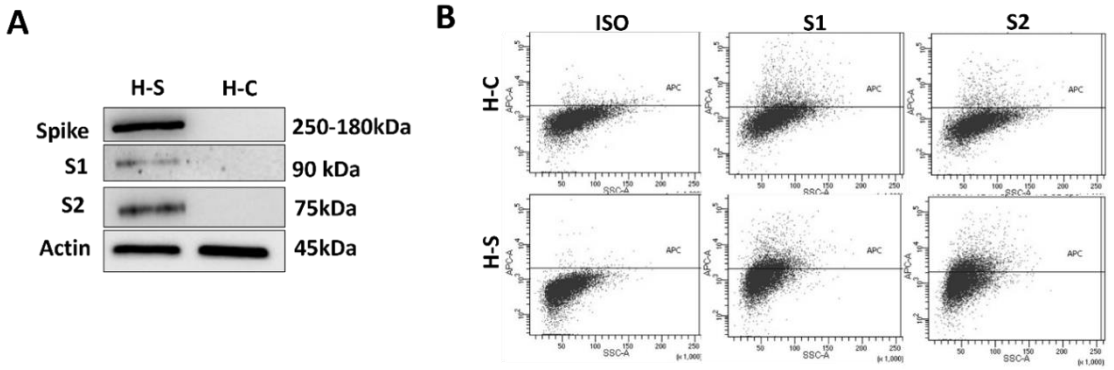

Figure 11. Analysis of S1 and S2 presence in H-S and H-C. (**A**) Western blot analysis of spike protein (250-180 kDa), the S1 (90 kDa) and S2 (75 kDa) in H-S and H-C. The actin protein (45KDa) was used as endogenous control. (**B**) Representative dot plot of Cytofluorimetric analysis for S1 and S2 subunits respect to the control isotype (ISO) in H-S and H-C.

Characterization of spike subunits on S-EVs

Once validated the S1 and S2 presence at level of H-S, we focused the subsequent analysis on spike subunits characterization on S-EVs. We used the MACSPlex analysis to obtain information about the S-EV positivity for S1 and S2 subunits. Specifically, we selected S-EVs using beads-Fitc-Pe positive covered with anti-tetraspanins (anti-CD9, anti-CD63 and anti-CD81). We plotted these positive beads-Fitc-Pe-EV population with their simultaneously positivity for anti-S1-APC and anti-S2-APC. The MACSPlex analysis revealed different vesicles populations, in particular: S-EVs positive only for S1 (S1-EVs), S2 (S2-EVs) or both (S1S2-EVs) subunits (Fig.12 A). All the different subpopulations were expressing tetraspanins (CD9, CD63 and CD81) and showed an homogenous surface renal progenitor markers pattern of expression (Fig.12 A). We confirmed, by western blot, the presence of S1 and S2 only in S-EV samples (Fig.12 B). In addition, with super resolution microscopy, we selected using CD63 the EV population and we demonstrated the coexpression of CD63 with both S1 or S2 on S-EVs (double or triple positive) and with size between 50 and 100 nm (Fig.12 C).

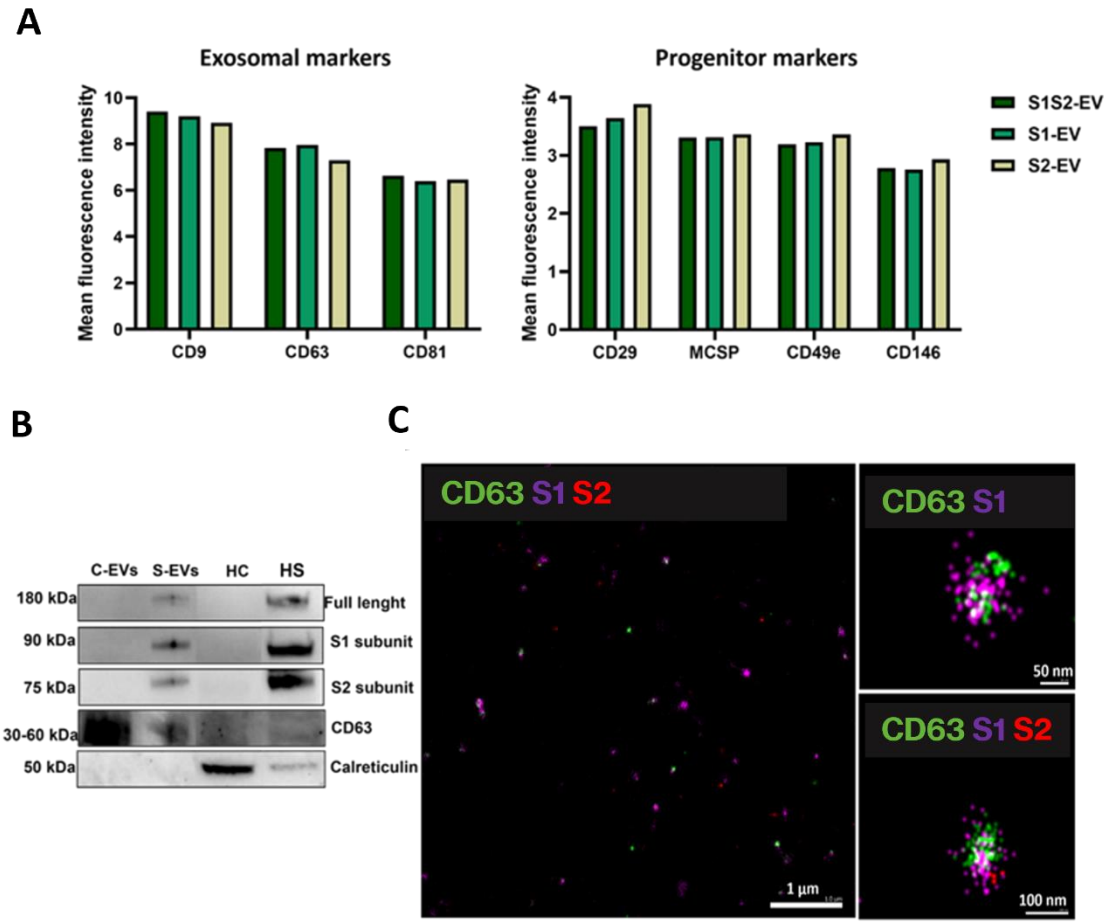

Figure 12. **Validation of S1 and S2 presence on S-EVs.** (**A**) Quantification of the median APC fluorescence for each bead population after background correction, clustered in exosomal and progenitor markers. The progenitor markers were normalized to median fluorescence intensity of all detectable markers. (**B**) Western blot images of spike full length (180 kDa), S1 (90 kDa), S2 (75 kDa) in C-EVs, S-EVs, H-C and H-S. CD63 was used as an exosomal marker and calreticulin as a negative EV marker. (**C**) Super-resolution microscopy micrographs showing the pattern distribution of CD63 in green, S1 in violet, S2 in red.

EV Interaction with cell membrane model

The SARS-CoV-2 spike interaction with recipient cell and in particular the role of membrane on the virus uptake are still lacking. In collaboration with the team of Prof. Loredana Casalis from the university of Trieste, we explored EV interaction with synthetic planar lipid bilayer with cholesterol designed to mimic the formation of raft-like nanodomains in cell membrane. Using Atomic Force Microscopy, we were able to track the EV interaction with a cell membrane model. We observed that after the S-

EV addition the lipid raft domains were not visible around the site of interaction compared to the C-EV interaction, meaning that either they were fluidified or recruited from the S-EVs (Fig. 13 A). S-EVs showed a major membrane area of interaction and with initial pore formation of supported lipid bilayer comparing to C-EVs (Fig. 13 B).

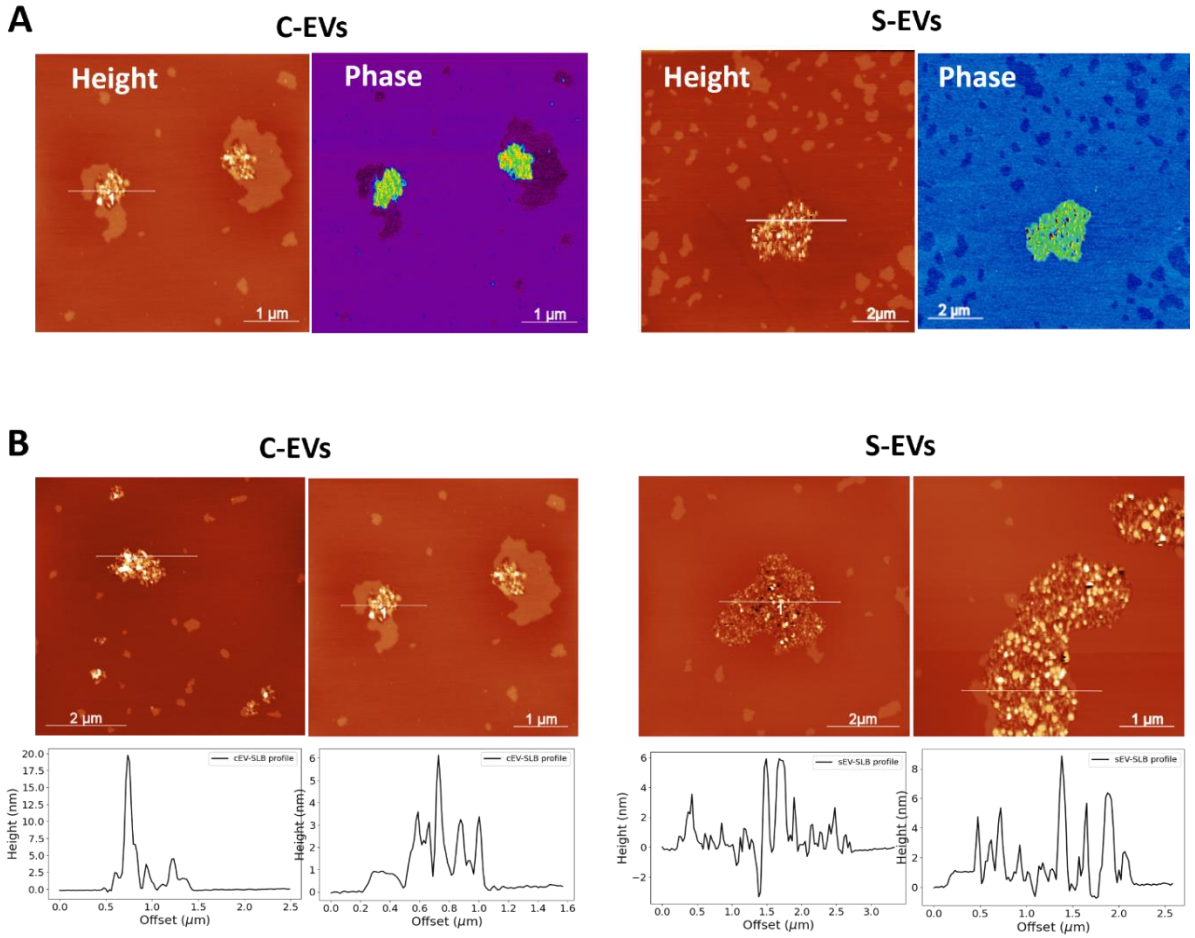

Figure 13. EV interaction with supported lipid bilayer (SLB). (**A**) Atomic force microscopy (AFM) topographic images of height or phase signal of DOPC/SM 2 : 1 (m/m) SLB with 10 mol% Cho with S/C-EV interaction at the level of liquid-ordered (L_o) domains. The height signal showed the distribution of lipid raft and the point of interaction; the phase signal showed the differences in composition: lipids (violet/blue) and EVs/proteins (green/yellow). (**B**) Time-resolved AFM topographic images of S/C-EVs interacting with DOPC/SM 2 : 1 (m/m) SLB with 10 mol% Chol with corresponding height profiles, acquired at 27 ◦C in Tris buffer 10 mM in 10 minutes.

Analysis of ACE2 expression

To evaluate the S-EV interaction with target cells, we analyzed the presence of ACE2 receptor on the cells. The cytofluorimetric analysis confirmed the ACE2 expression on endothelial (HUVEC) and epithelial bronchial cells (16HBE14o-) respect to the MRC5 (0,4% positive for ACE2), used as negative control. In particular, HUVEC and 16HBE14o- expressed 36,8 % and 31,6 % ACE2 positive cells, respectively (Fig.14). HK2 and G7 cells showed a very low expression for ACE2, 7,4% and 5%, and considered negative (Fig. 14). Subsequently, we evaluated the EV uptake in ACE2 positive or negative cells.

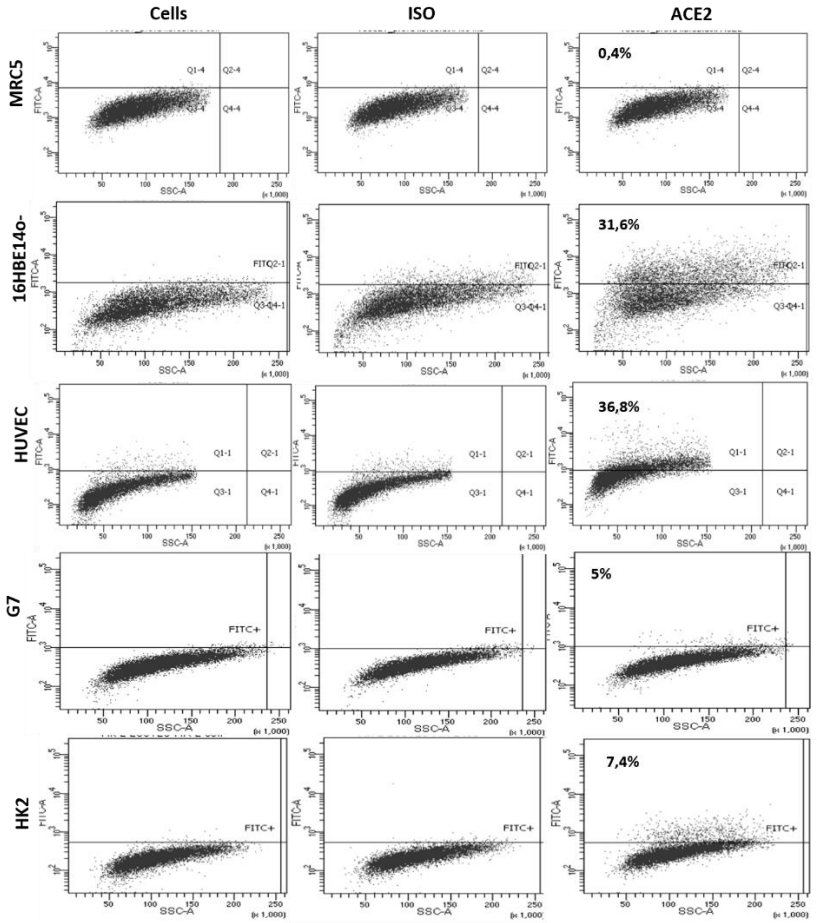

Figure 14. ACE2 expression. Representative dot plots of cytofluorimetric analysis of ACE2 receptor on human fibroblast (MRC5) used as a negative control that showed the control isotype staining (ISO), on human bronchial epithelial cells (16HBE14o-), on human umbilical vein (HUVEC), on human renal cancer stem cells (G7) and on human renal proximal tubular cells (HK-2).

S-EVs uptake by ACE2 positive cells

The endothelial activation and dysfunction participate in COVID-19 pathogenesis by altering the integrity of vessel barrier, promoting pro-coagulative state, inducing endothelial inflammation and leukocyte infiltration [75],[76]. Therefore, we focused on the S-EV/HUVEC interaction. In addition, we analyzed the S-EV uptake by a bronchial epithelial cell line 16HBE14o-, SARS-CoV-2 virus target cells [77]. Once demonstrated and confirmed the ACE2 (spike receptor) expression by HUVEC and 16HBE14o-, we analyzed the possible interaction of S-EVs with target cells. We demonstrated a time dependent uptake of fluorescently labeled S-EVs or C-EVs by HUVEC. S-EVs were more internalized than the C-EVs, in each experimental time point considered, as detected by the immunofluorescence analysis (Fig. 15 A). The best time chosen for the EV uptake was 3 hours. Comparing the uptake of S-EVs and C-EVs, after 3 hours, we confirmed a significant higher entrance of S-EV with respect to the C-EVs in both target cells (HUVEC and 16HBE14o-), quantified by cytofluorimetric analysis (Fig. 15 B, C). These data supported the major interaction of S-EVs compared to C-EVs with supported lipid bilayer previously observed (Fig. 13).

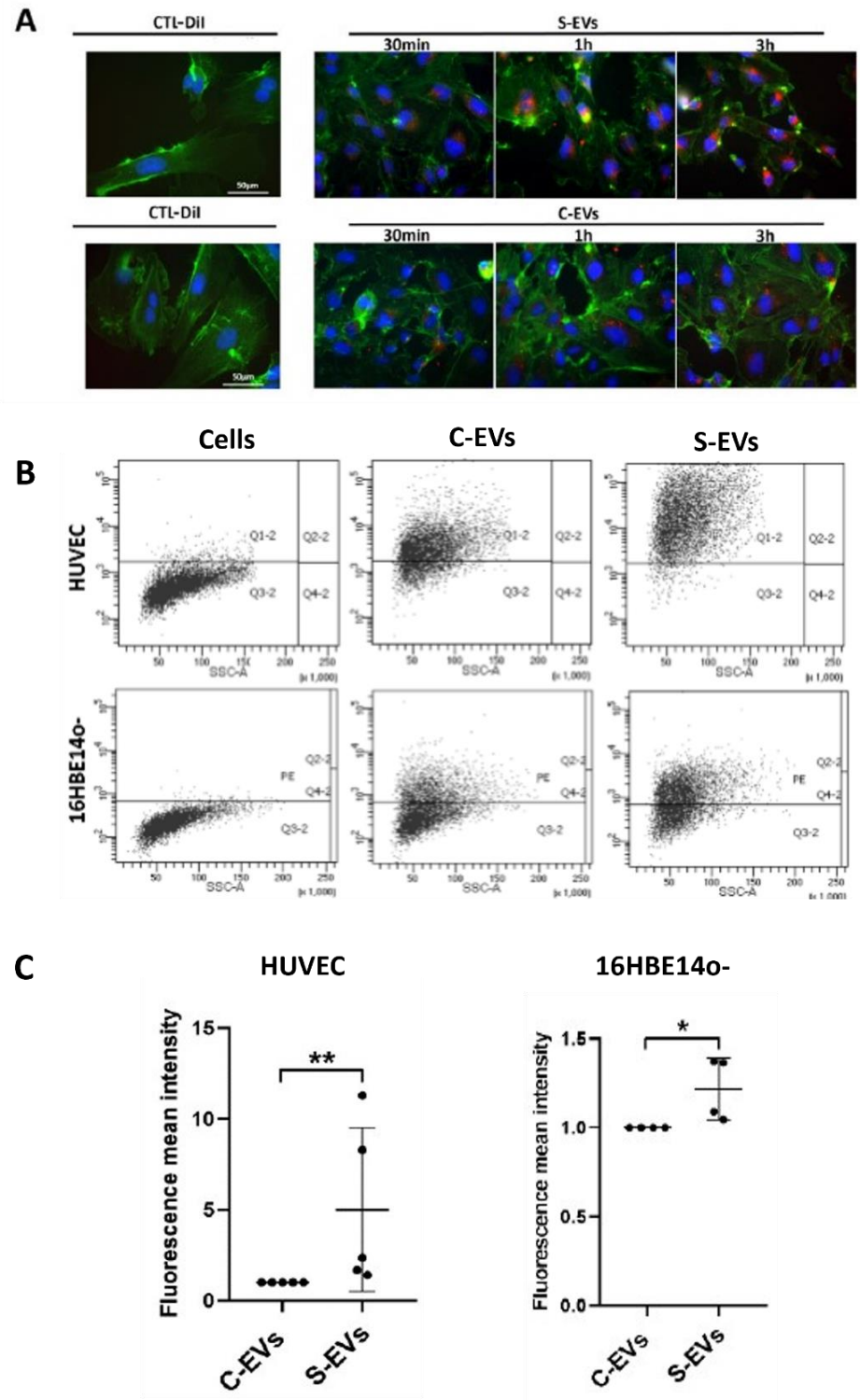

Figure 15. **EV uptake by ACE2 positive cells.** (**A**) Representative immunofluorescence micrograph of S-EV or C-EV uptake by HUVEC after 30min (S/C-EVs 30min), 1hour (S/C-EVs 1h) or 3hours (S/C-EVs 3h) respect to the control (CTL). Cells were stained with FITC-phalloidin (green), nucleus stained with the DAPI (blue), EVs were labeled with DiI (red); magnification 40×. (**B**) Representative flow cytometry dot plots of only cells (without EV treatment) and of S-EV or C-EV uptake by HUVEC and 16HBE14o-. (**C**) Fluorescence mean intensity of all positive events obtained by cytofluorometric analysis. Data were normalized to the respective uptake control (S-EVs or C-EVs), set as one, used as a reference sample for each experiment. The unpaired t-test was performed after the normalization for C-EV vs. S-EV uptake with * $p < 0.05$, **$p<0,01$. The graphs show the average of at least four independent experiments ± SD. Figure modified from Verta, Roberta et al. "Generation of Spike-Extracellular Vesicles (S-EVs) as

a Tool to Mimic SARS-CoV-2 Interaction with Host Cells." Cells vol. 11,1 146. 3 Jan. 2022, doi:10.3390/cells11010146.

S-EVs uptake by ACE2 negative cells

Demonstrated that G7 and HK-2 cells were ACE2 negative (Fig.14), we investigated the S-EV and C-EV uptake in these cells. With cytofluorimetric analysis, we noted that C-EVs were significantly internalized more in comparison to the S-EVs (Fig. 16), in contrast to what we observed previously considering the EV uptake by HUVEC and 16HBE14o-, ACE2 positive (Fig. 15 A, B). These results demonstrated that the S-EV entrance is ACE2 dependent by ACE2 receptor expression on the target cells.

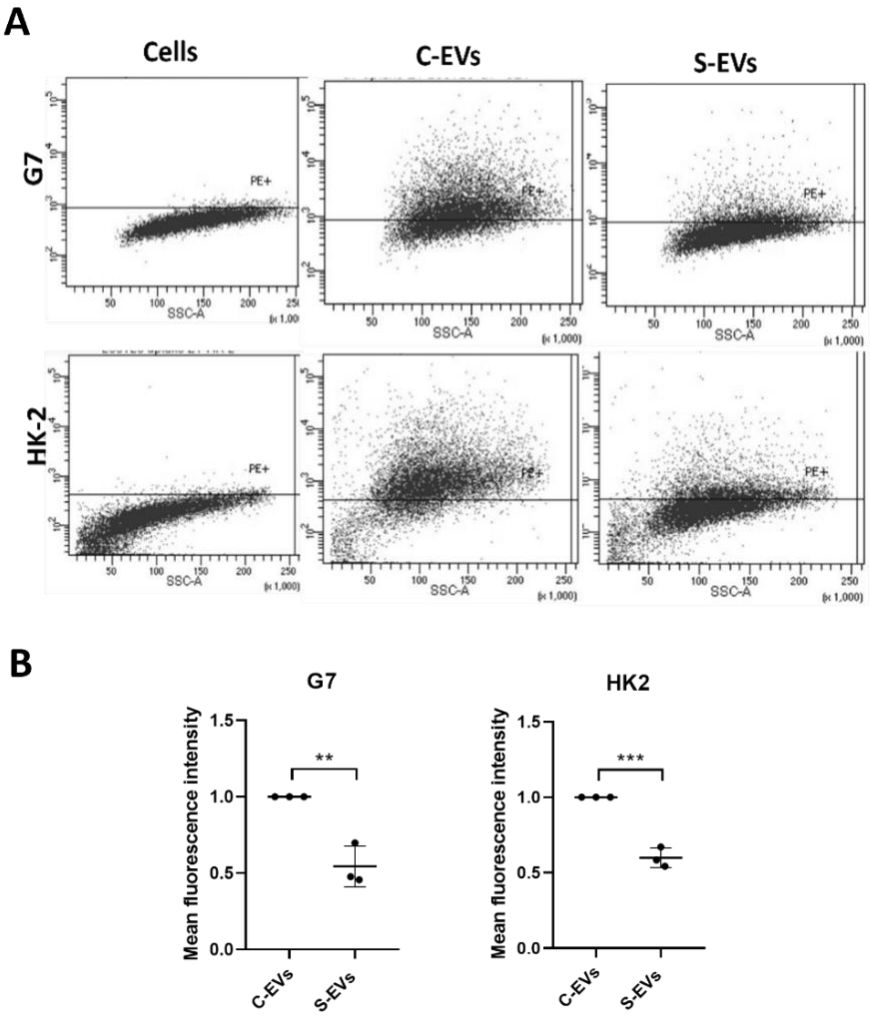

Figure 16. Analysis of EV uptake by ACE2 negative cells. (**A**) Representative flow cytometry dot plots of only cells (without EV treatment) and of S-EV or C-EV uptake by G7 and HK2. (**B**) Fluorescence

mean intensity of all the positive events obtained by the cytofluorometric analysis. Data were normalized respect to C-EVs for both the EV uptake analysis by G7 and HK-2. The Unpaired t-test was performed after the normalization for C-EV vs S-EV uptake with **p <0.01 or ***p <0.001. The graphs show the average of at least three independent experiments ± SD.

Modulation of S-EV uptake by ACE2 blocking antibody

To confirm previous results, on spike-ACE2 dependent interaction (Fig. 15 and Fig. 16), we analyzed the EV uptake by target cells with the presence of ACE2-blocking antibody. The ACE2 blocking antibody was able to significantly reduce the S-EV uptake by HUVEC, but not in the case of C-EVs (Fig. 17 A, B). We also monitored the EV internalization by bronchial epithelial cells (16HBE14o-) with the anti-ACE2 pre-treatment. We validated the significant reduction only of S-EV uptake by ACE2 blocking antibody also using 16HBE14o- (Fig. 17 C, D). Our results support the S-EV binding to target cells through an ACE2 dependent-interaction, in the same manner as the SARS-CoV-2 virus. As S-EVs mimic SARS-CoV-2 interaction with host cells, it appears as an important resource in this scenario in identifying new therapeutic strategies.

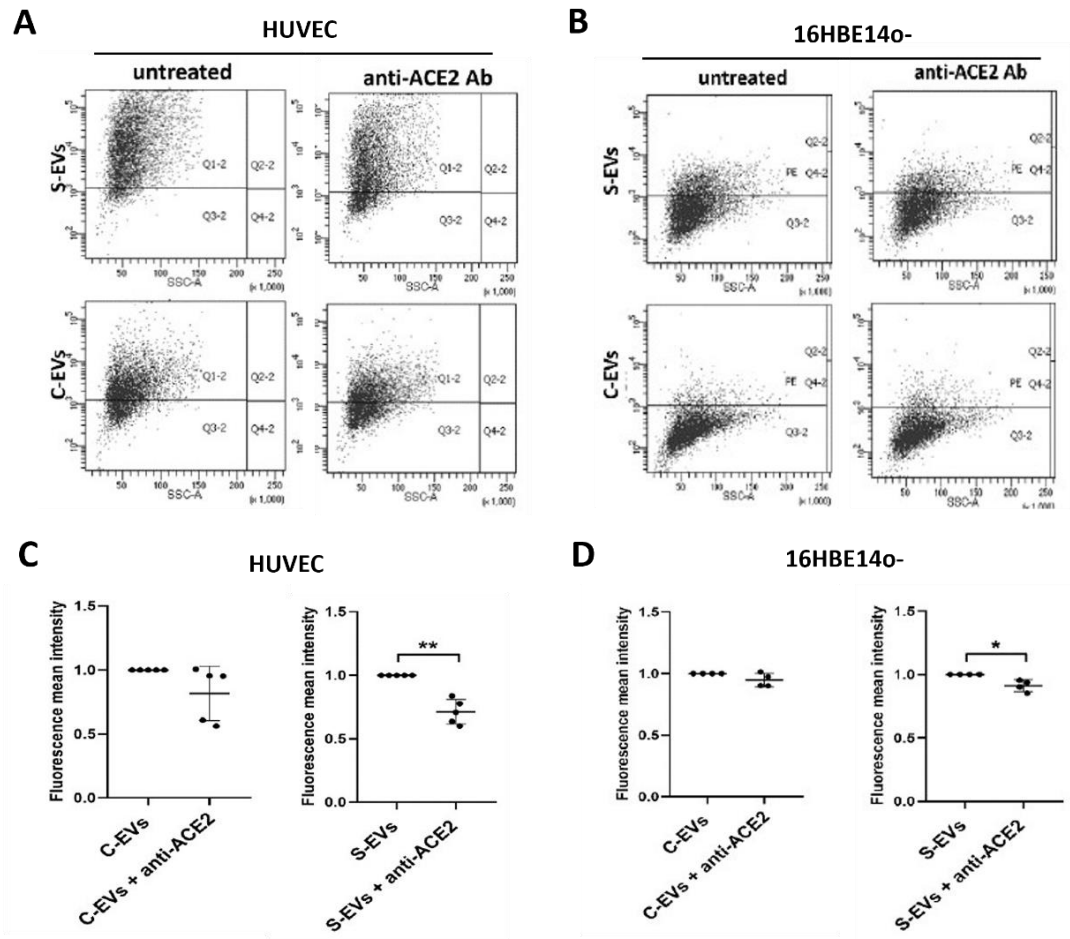

Figure 17. Effect of anti-ACE2 blocking antibody on the EV uptake by the endothelial cells (HUVEC) and bronchial epithelial cells (16HBE14o-). (**A**) Representative flow cytometry dot plots of S-EV or C-EV uptake by HUVEC without treatments (untreated) or anti-ACE2 20 µg/mL (S/C-EVs anti-ACE2 Ab). (**B**) Representative flow cytometry dot plots of S-EV or C-EV uptake by 16HBE14o- without treatments (untreated) or anti-ACE2 20 µg/mL (S/C-EVs anti-ACE2 Ab). (**C**) Fluorescence mean intensity of all positive events obtained by cytofluorometric analysis of HUVEC. (**D**) Fluorescence mean intensity of all positive events obtained by cytofluorometric analysis of 16HBE14o-. For the comparison EVs + anti-ACE2, data were normalized to the EVs. The paired t-test was performed after the normalization for untreated EVs vs. EVs + treatments with * $p < 0.05$, ** $p < 0.001$. The graphs show the average of at least four independent experiments ± SD. Figure modified from Verta Roberta et al. "Generation of Spike-Extracellular Vesicles (S-EVs) as a Tool to Mimic SARS-CoV-2 Interaction with Host Cells." Cells vol. 11,1 146. 3 Jan. 2022, doi:10.3390/cells11010146.

Modulation of virus like particle and tumor-EV uptake by Colchicine treatment

Colchicine, a microtubule antagonist that inhibits the tubulin polymerization [78],[79], is widely used in various pathologies such as gout, familial mediterranean fever and rheumatoid arthritis [52],[55],[56] due to its involvement in several anti-inflammatory pathways. Recently, studies considered colchicine as a clinical trial for COVID-19

treatment [57], [58]. Microtubules are considered an ideal target for anticancer drugs because of their essential role in mitosis [61], therefore colchicine seems to be, also, promising for cancer therapy [54],[56],[61],[62].

We observed that colchicine altered the HUVEC shape and induced the loss of adhesiveness between cells, while remain unaltered the cell morphology after ACE2 blocking antibody treatment (Fig. 18 A). In parallel, colchicine significantly reduced the S-EV internalization, with a trend of reduction also for the C-EV uptake by HUVEC (Fig. 18 A, B, D). Comparable results were observed on bronchial epithelial cells. Colchicine significantly decreased the S-EV and the C-EV uptake by 16HBE14o- (Fig. 18 C, E).

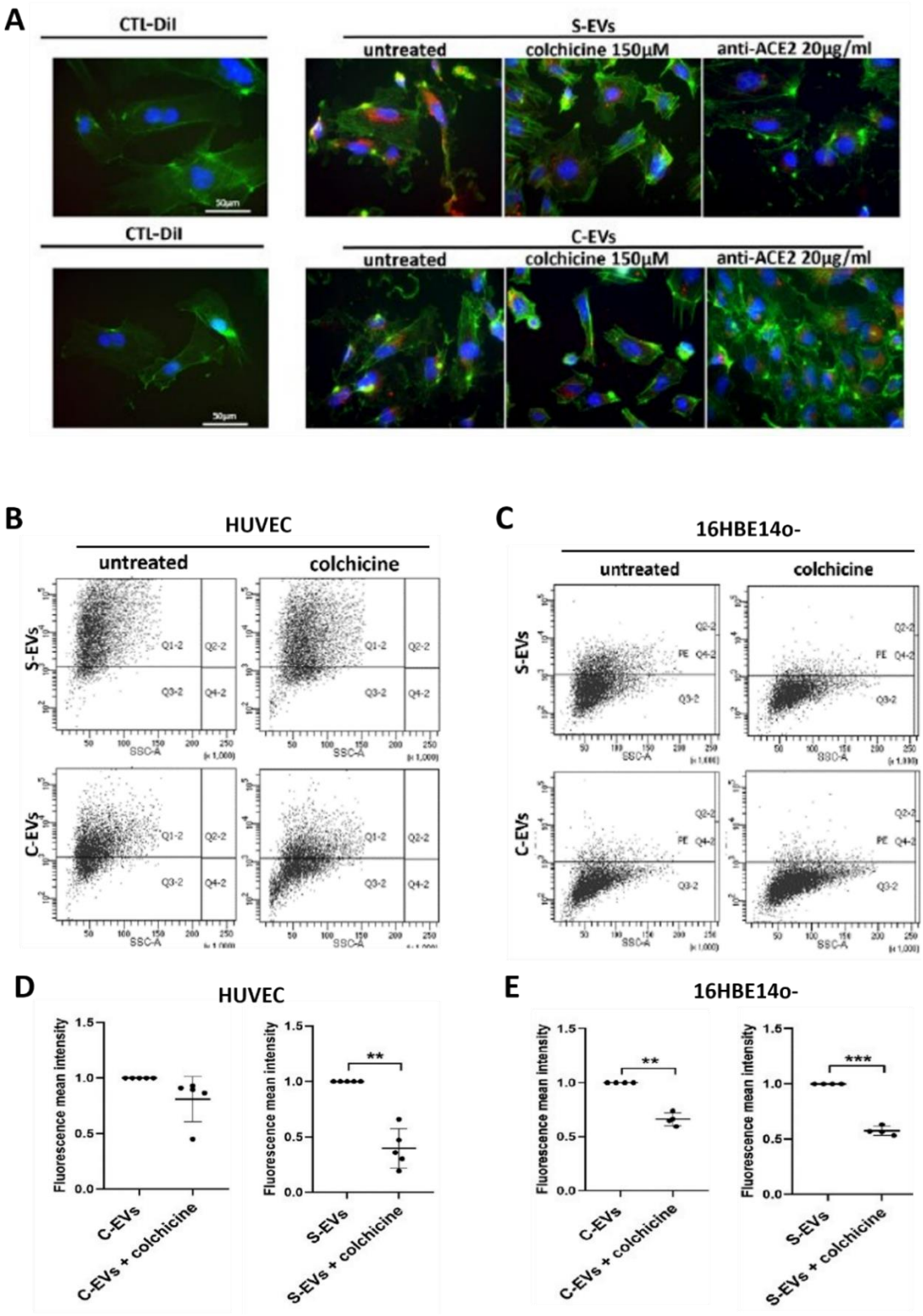

Figure 18. Effect of colchicine on the EV uptake by human umbilical vein endothelial cells (HUVEC) and bronchial epithelial cells (16HBE14o-). (**A**) Representative immunofluorescence micrograph of S-EV or C-EV uptake modulation by HUVEC with colchicine or anti-ACE2 blocking antibody with respect to the uptake without treatments (untreated) or to control (CTL-DiI), prepared with DiI control solution in the absence of EVs. Cells were stained with FITC-phalloidin (green), nucleus-stained with DAPI (blue), EVs were labeled with DiI (red); magnification x40. (**B**) Representative flow cytometry dot plots of S-EV or C-EV uptake by HUVEC without treatments (untreated) or with colchicine 150µM (S/C-EVs + colchicine). (**C**) Representative flow cytometry dot plots of S-EV or C-EV uptake. (**D**) Fluorescence mean intensity of all the positive events obtained by the cytofluorometric analysis on

HUVEC. (**E**) Fluorescence mean intensity of all the positive events obtained by the cytofluorometric analysis on 16HBE14o-. Data were normalized to the respective uptake control (S-EVs or C-EVs), set as 1, used as a reference sample for each experiment. For the comparison C-EVs vs C-EVs + colchicine data were normalized to the C-EVs. For the comparison S-EVs vs S-EVs + colchicine data were normalized to the S-EVs. The Paired t-test was performed after the normalization with ** $p<0.01$, ***$p<0,001$. The graphs show the average of at least four independent experiments ± SD. Figure modified from Verta, Roberta et al. "Generation of Spike-Extracellular Vesicles (S-EVs) as a Tool to Mimic SARS-CoV-2 Interaction with Host Cells." Cells vol. 11,1 146. 3 Jan. 2022, doi:10.3390/cells11010146.

To explore the potential effect of colchicine on EV uptake inhibition, we isolated and characterized EVs from tumor, specially, from ovarian cancer and colorectal cancer cells (SKOV3 and HT29) and we assessed the tumor-EVs entrance in human microvascular endothelial cells (HMEC) and the human renal cancer endothelial cells (EcK) after colchicine treatment. The nanoparticle tracking analysis showed that we obtained tumor-EVs with size around 100nm (Fig. 19 A, C), the MACSPlex analysis confirmed the exosomal identity by the expression of vesicular markers on tumor-EVs and some progenitor markers (Fig.19 B, D). Specifically, CD63 is the major tetraspanins expressed on SKOV3-EVs, while HT29-EVs expressed quite homogenously CD9, CD63 and CD81. Both the tumor-EVs population were positive for CD29, CD44 and CD24 (Fig.19 B, D). Among the progenitor markers the analysis revealed the major expression of CD142, SSEA-4 on SKOV3-EVs and ROR1, CD326, CD133-1 on HT29-EVs (Fig.19 B, D).

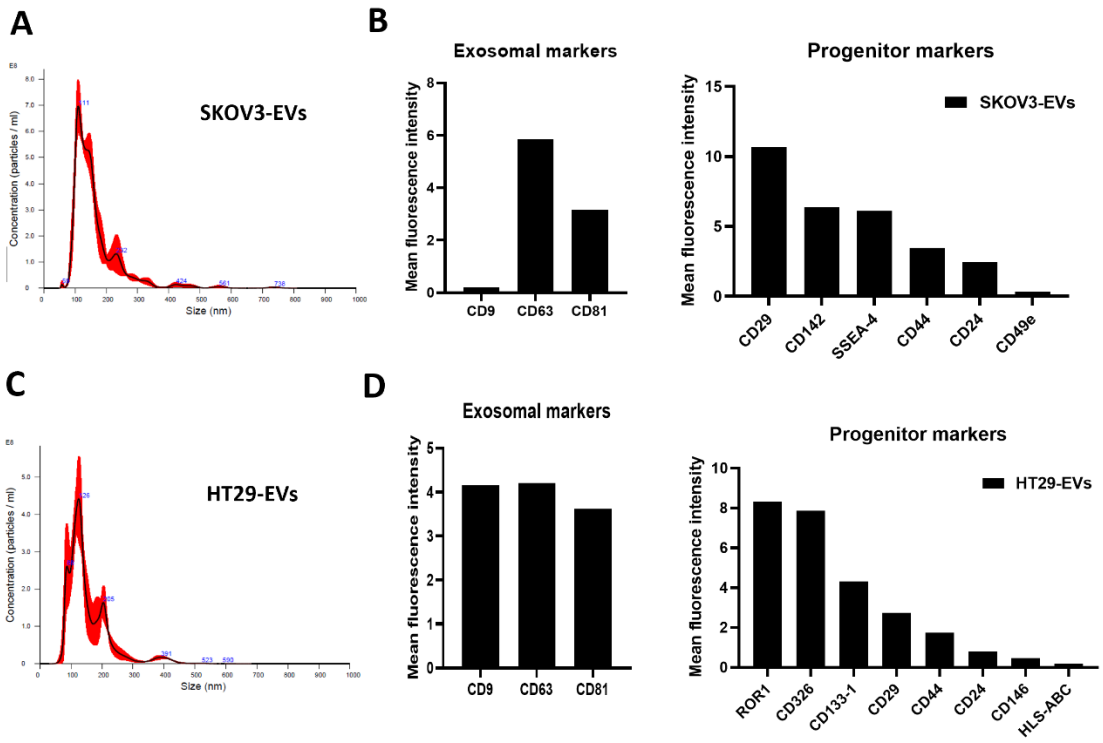

Figure 19. Characterization of SKOV3-EVs and HT29-EVs. (**A**) Representative nanoparticle tracking analysis of EVs from ovarian adenocarcinoma (SKOV3-EVs) showing EV size distribution. (**B**) Quantification of the median APC fluorescence of SKOV3-EVs for each bead population after background correction, clustered in exosomal and progenitor markers. (**C**) Representative nanoparticle tracking analysis of EVs from colorectal cancer cells (HT29-EVs) showing EV size distribution. (**D**) Quantification of the median APC fluorescence of HT29-EVs for each bead population after background correction, clustered in exosomal and progenitor markers. Data were normalized to median fluorescence intensity of all detectable markers.

It was demonstrated that tumor-EVs are responsible of metastasis and angiogenesis, mechanisms involved in cancer development [80],[81]. The colchicine pretreatment was able to reduce significantly both the tumor-EV (SKOV3-EVs and HT29-EVs) uptake by HMEC (Fig. 20 A, C.) and EcK (Fig. 20 B, D) in comparison to endothelial cells subjected only to tumor-EV stimulation but without colchicine treatment (Fig. 20). These results demonstrated that colchicine seems to be promising to reduce the tumor-EV internalization by physiological and cancer endothelium, mechanisms that can be responsible of tumor progression [82].

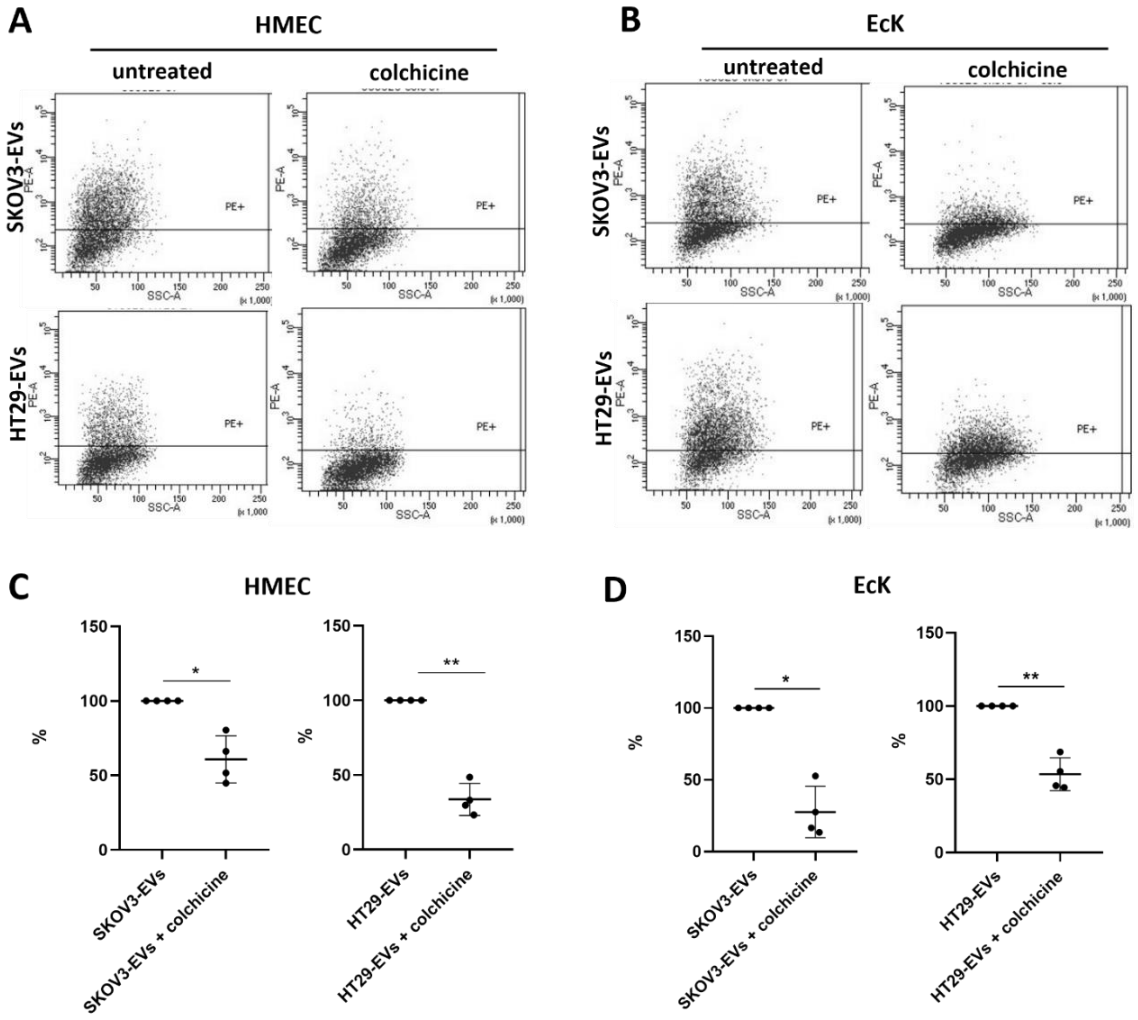

Figure 20. Colchicine modulation of tumor-EV uptake by HMEC and EcK. (**A**) Representative flow cytometry dot plots of SKOV3-EV or HT29-EV uptake by HUVEC without treatment (untreated) or with colchicine 150μM (SKO3/HT29-EVs + colchicine). (**B**) Representative flow cytometry dot plots of SKOV3-EV or HT29-EV uptake by Eck without treatment (untreated) or with colchicine 150μM (SKO3/HT29-EVs + colchicine). (**C**) The percentage (%) of all the positive events obtained by the cytofluorometric analysis on HMEC. (**D**) The percentage (%) of all the positive events obtained by the cytofluorometric analysis on EcK. Data were normalized to the respective uptake control (SKOV3-EVs or HT29-EVs), set as 100%, used as a reference sample for each experiment. For the comparison SKOV3-EVs vs SKOV3-EVs + colchicine data were normalized to SKOV3-EVs. The Paired t-test was performed after the normalization with * $p<0.05$ or ** $p<0,01$. For the comparison HT29-EVs vs HT29-EVs + colchicine data were normalized to HT29-EVs. The Paired t-test was performed after the normalization with * $p<0.05$ or ** $p<0,01$. The graphs show the average of at least four independent experiments ± SD.

Discussion

EVs are known to be involved in the pathogenesis of several diseases such as in infections and cancer [83],[84]. Moreover, EVs and viruses share common aspects: size, structure, biogenesis, uptake and ability to carry a specific cargo while being different entities [32],[33]. The interesting interaction between EVs and the viruses open a new perspectives on treatment of COVID-19 [39].

B. Krishnamachary et al. in 2021 observed that EVs isolated from plasma of patients with COVID-19 were significantly loaded, at different expression levels, with cardiovascular and inflammatory proteins, according to the severity of disease [41]. In parallel, C. Balbi et al. (2021) demonstrated that, during the SARS-CoV-2 infection, the systemic inflammatory response results in cell-release of substantial amounts of procoagulant EVs that may act as clotting initiation agents, contributing to COVID-19 progression. EVs also contribute significantly to the transmission of viral infections, as highlighted by K. Owczarek et al. (2018) [85]. EVs may contribute to the infection, internalization, and transmission of SARS-CoV-2 virus because of some components (such as miRNAs, viral proteins and viral receptor ACE2) that could be packed into EVs, that render the recipient cells sensitive to viral invasion [86].

The SARS-CoV-2 infection begins with the virus binding to ACE2 [6],[18] and the virus entrance into host cells is mediated by the spike glycoprotein that is composed of two functional subunits, the S1 and S2 [6],[18].

The S1 subunit consists of an N-terminal domain and a receptor binding domain and acts to bind to the receptor on the host cell. The S2 subunit subsequently fuses the virus-cell membranes [4],[5],[87]. The spike glycoprotein is crucial for the entry of SARS-CoV-2 and represents an excellent target for anti-viral therapeutic development.

Therefore, the aim of this study was to generate and characterize EVs expressing the spike protein of SARS-CoV-2, with indirect engineering method, using HEK-293T-Spike-transfected cells, as a model to study the virus interaction with target cells in normal conditions or in presence of new possible pharmacological treatments.

By TEM and NTA, we demonstrated that we obtained intact vesicles with size around 100nm. The western blot analysis revealed the presence of spike protein only in EVs isolated from transfected cells with the spike expressing vector. The S-EVs were further characterized by MACSPlex, confirming the exosomal markers expression and their cell origin by the presence of renal progenitor markers on EV surface. Subsequently, S-EVs were analyzed at single EV level using ExoVieW and super resolution microscopy. These analyses confirmed the presence of spike protein and its co-expression with tetraspanins (CD9, CD63 and CD81). Moreover, the super resolution microscopy analysis proved the S-EV dimension observed, previously, by TEM and NTA.

The EV engineering with viral elements, due to the EV similarities with viruses, is a promising and interesting scenario for the scientific community, especially for anti-viral purposes. A recent study demonstrated that ACE2-engineered EVs limit the SARS-CoV-2 infection [46]. Another work showed the possibility of producing EVs expressing the receptor-binding domain (RBD) of the viral spike protein, that recognizes ACE2 receptor, to be used as a target delivery system of potential anti-viral agents *in vivo* [49].

In our study, once we demonstrated the spike presence on EV surface, we decided to investigate on spike subunits (S1 and S2) characterization. We obtained S-EVs positive for one subunit (S1-EVs or S2-EVs) or for both (S1S2-EVs) and these results offer new perspectives. We can take advantage of using S1-EV for diagnostic, for their

capacity to recognize specifically the ACE2 receptor, independently from the presence of S2.

We know that different tumors overexpress ACE2, such as colorectal adenocarcinoma, renal carcinoma, pancreatic and lung adenocarcinoma [88].

In the future, it will be possible to consider the use of S1-EVs to recognize tumor cells to estimate the tumor size and presence of metastasis. While the S1S2-EVs can be useful for cargo-delivery studies in target site, using the S1-ACE2 specific interaction plus the fusogenic capacity of S2 subunit.

Therefore, it might be useful to separate our S-EV subpopulations to further investigate the different theragnostic potential of S1-EVs *vs* S1S2-EVs.

The S-EVs seem to be promising in diagnostic scenario and for the development of innovative therapies (drug delivery) or vaccines.

A parallel study, based on spike-EV production, showed that EVs containing SARS-CoV-2 spike interact with the humoral immune system and reduce serum neutralizing antibodies of convalescent patients [89]. In contrast, it was reported that mRNA-based vaccines against the SARS-CoV-2 virus infection devised by Pfizer and Moderna [90],[91] can generate circulating EVs carrying the SARS-CoV-2 S protein and promoting the generation of anti-S neutralizing antibodies in vaccinated healthy individuals [92].

Following the spike characterization, we observed the different involvement and mechanism of interaction of S-EVs compared to C-EVs on cell membrane model, using supported lipid bilayer. Specifically, S-EVs revealed a major surface membrane area of interaction and with initial formation of pores on the supported lipid bilayer, a possible fusogenic mechanism. It seems that spike protein plays a role on membrane perturbation, a process that can promote the spike interaction with host cell receptor. It is unclear which spike subunit (S1/S2) is involved or if it is a specific protein domain

that controls this mechanism. A limit of our study may be the heterogeneity within the S-EV population (S1-EVs, S2-EVs, S1S2-EVs) that does not allow us to distinguish which one of spike subunits appears to be specifically responsible for the cell membrane perturbation. Therefore, the addition of anti-S1 or anti-S2 during the S-EVs interface with supported lipid bilayer, could be helpful to understand the specific mechanism of spike subunit interaction with the cell membrane.

A recent study demonstrated that SARS-CoV-2-S1 can destabilize the cellular membrane independently by the target receptor [93],[94]. While previously, Guillén J. and colleagues (2008) showed the role of SARS-CoV-S2 subunit in cell membrane perturbation [95]. These dynamic changes of cell membrane facilitate the spike-receptor binding [96]. Interestingly, we tested our S-EVs on a cell membrane model with cholesterol. The cholesterol-enriched rafts represent a center for the recruiting of specific SARS-CoV-2 receptors that can facilitate the virus fusion with the host cell membrane and promoting virus entry [95],[96],[97],[98].

Consequently, to evaluate the specificity of spike-ACE2 receptor binding on the virus target cells, we performed the cytofluorimetric analysis to investigate the EV entrance in cells positive or negative for ACE2. We focused on human bronchial epithelial cells (16HBE14o-), that represent the first site of SARS-CoV-2 virus infection [99],[100] and on endothelial cells (HUVEC) that are involved in the development of SARS-CoV-2 pathology [75],[76].

S-EVs were significantly more internalized by ACE2 positive cells (HUVEC e 16HBE14o-) in respect to control EVs, without the spike (C-EVs). Conversely, we observed a significative increase in the uptake of C-EVs in ACE2 negative cells (G7 e HK-2). These data support that the S-EV interaction with host cell is ACE2 dependent and the spike could act as an additional factor for EV uptake, supporting its primary role in the virus–host interaction [76].

It is essential to underline that our study did not take advantage of using cells that overexpress ACE2, but it was tested the interaction between virus-like particles and the basal ACE2 receptor expression on target cells.

In contrast to what we observed, Choi and colleagues in 2022 showed that EVs expressing spike labelled with green fluorescent protein (EV-S-GFP) were not internalized but remain attached on the surface of cell membrane [101]. This probably happened because the GFP presence on EV surface can create a steric hindrance that hampers the correct and complete spike interaction with the target host cell receptor.

Our results, on spike-ACE2 dependent interaction, were further confirmed by the presence of anti-ACE2 blocking antibody that modulates the S-EV entrance into endothelial and bronchial epithelial cells. S-EV uptake into target cells was reduced significantly by anti-ACE2.

Given that S1 acts to bind ACE2 on target cell, S2 fuses the virus-cell membranes [18], S-EVs showed a peculiar and greater interaction than C-EVs with cell membrane model and since we observed a significant major internalization of S-EVs by target cell, therefore we believe that it might be useful, in the future, to investigate the S-EVs role on endosomal escape evaluating, in parallel, the S-EV efficiency on cargo-delivery in target site.

Currently, there is not specific therapeutic for COVID-19 [26]. The treatment strategies improved patient recovery and survival but they do not definitively restore lung damage caused by the virus. In addition, a range of anti-inflammatory drugs have been tested to inhibit the cytokine storm and multiple organ failure caused by the worsening immune response in severe patients, but the effect has not been significant [26].

To evaluate a new possible therapeutic strategy to contrast SARS-CoV-2 infection, we also analyzed the modulation of S-EV and host cell interaction using colchicine.

Colchicine, a microtubule antagonist, is an anti-inflammatory drug that may contrast the COVID-19 disease with different mechanisms. The rationale for the use of colchicine in COVID-19 is based on its well-known anti-inflammatory, anti-fibrotic properties and its theoretical antiviral action, indirectly supported by the role of microtubules for the entry of the human coronavirus [102],[103]. This interference with microtubule polymerization influences the macrophage diapedesis, endocytosis, and exocytosis, and consequently the interleukins (ILs) production [104],[105],[106]. Recently, it has been shown how colchicine inhibits the NOD-like receptor family pyrin domain containing 3 (NLRP3) inflammasome, possibly through its microtubule antagonism [107] and therefore blocks the IL-1 and IL-18 formation [108],[109],[110]. In addition, colchicine showed an impressively rapid effect on endothelial hyper-permeability observed in the capillary leak syndrome [60].

In this study we noted a significant reduction in S-EV and C-EV uptake into HUVEC and 16HBE14o- after colchicine treatment. The EV uptake inhibition, observed in both EV populations, can be explained by the direct effect of colchicine on cell cytoskeleton and consequently this can cause an indirect effect on cell membrane capacity to interact and to internalize the EVs.

These data demonstrated that EVs expressing SARS-CoV-2 spike protein can be a replicable and safe virus like particle model that mimics SARS-CoV-2 virus.

Interestingly, colchicine treatment was able to prevent S-EV entry with a stronger effect than that of ACE2 neutralizing antibody. Moreover, it also prevented the entry of C-EVs into cells, in particular into bronchial epithelial cells, suggesting an additional effect due to activity on microtubules and cell cytoskeleton. This is an example of recipient cell modulation, an indirect method to modulate the EV cellular uptake. This aspect is of interest for further studies aimed at blocking EV entry in pathologies involving EV-mediated spread of the disease. In the last part of this study, we explored the colchicine

effect on EV entrance into endothelial cells, using EVs derived from human ovarian adenocarcinoma cells (SKOV3-EVs) and human colorectal cancer (HT29-EVs). Interestingly, we also demonstrated the inhibition of both tumor-EV entrance in HMEC and EcK in the presence of colchicine in comparison to untreated cells.

Conclusions

The development of effective vaccines, therapeutics, and drug delivery systems to the target site is a field that has increasingly gained attention to overcome SARS-CoV-2. This work demonstrates the possibility to generate and to use of S-EVs as a safe method for the study of COVID-19 and for the development of new therapeutic strategies. S1-EVs could be useful for diagnostic purposes thanks to specific ACE2 interaction, whereas S1S2-EVs could be employed for drug delivery to target cells (ACE2 positive). These results open the door to new future scenarios in theragnostic applications, allowing to overcome the problems related to the endosomal degradation of EVs which represent a potential limit for EV-based therapies. Finally, we identified a new pharmacological tool to modulate EV entry, that deserves further studies for possible application not only in SARS-CoV-2 infection, but also in oncology.

References

1. Lamers, M.M.; Haagmans, B.L. SARS-CoV-2 pathogenesis. *Nat. Rev. Microbiol.* **2022**, *20*, 270–284, doi:10.1038/s41579-022-00713-0.

2. Lui, G.; Guaraldi, G.; Lui, G. Drug treatment of COVID-19 infection. *Curr. Opin. Pulm. Med.* **2023**, *29*, 174–183, doi:10.1097/MCP.0000000000000953.

3. Benton, D.J.; Wrobel, A.G.; Xu, P.; Roustan, C.; Martin, S.R.; Rosenthal, P.B.; Skehel, J.J.; Gamblin, S.J. Receptor binding and priming of the spike protein of SARS-CoV-2 for membrane fusion. *Nature* **2020**, *588*, 327–330, doi:10.1038/s41586-020-2772-0.

4. Kumar, S.; Nyodu, R.; Maurya, V.K.; Saxena, S.K. Morphology, Genome Organization, Replication, and Pathogenesis of Severe Acute Respiratory Syndrome Coronavirus 2 (SARS-CoV-2). **2020**, *2*, 23–31, doi:10.1007/978-981-15-4814-7_3.

5. Sternberg, A.; Naujokat, C. Structural features of coronavirus SARS-CoV-2 spike protein: Targets for vaccination. *Life Sci.* **2020**, *257*, 118056, doi:10.1016/j.lfs.2020.118056.

6. Hoen, E.N.; Cremer, T.; Gallo, R.C.; Margolis, L.B. Extracellular vesicles and viruses: Are they close relatives? *Proc. Natl. Acad. Sci. U. S. A.* **2016**, *113*, 9155–9161, doi:10.1073/pnas.1605146113.

7. Akbari, A.; Rezaie, J. Potential therapeutic application of mesenchymal stem cell-derived exosomes in SARS-CoV-2 pneumonia. *Stem Cell Res. Ther.* **2020**, *11*, 1–10, doi:10.1186/s13287-020-01866-6.

8. Hu, B.; Guo, H.; Zhou, P.; Shi, Z.L. Characteristics of SARS-CoV-2 and COVID-19. *Nat. Rev. Microbiol.* **2021**, *19*, 141–154, doi:10.1038/s41579-020-00459-7.

9. Kaul, D. Since January 2020 Elsevier has created a COVID-19 resource centre with free information in English and Mandarin on the novel coronavirus COVID-19 . The COVID-19 resource centre is hosted on Elsevier Connect , the company ' s public news and information. **2020**, *10*, 54–64.

10. Cuervo, N.Z.; Grandvaux, N. Ace2: Evidence of role as entry receptor for sars-cov-2 and implications in comorbidities. *Elife* **2020**, *9*, 1–25,

doi:10.7554/eLife.61390.

11. da Rosa Mesquita, R.; Francelino Silva Junior, L.C.; Santos Santana, F.M.; Farias de Oliveira, T.; Campos Alcântara, R.; Monteiro Arnozo, G.; Rodrigues da Silva Filho, E.; Galdino dos Santos, A.G.; Oliveira da Cunha, E.J.; Salgueiro de Aquino, S.H.; et al. Clinical manifestations of COVID-19 in the general population: systematic review. *Wien. Klin. Wochenschr.* **2021**, *133*, 377–382, doi:10.1007/s00508-020-01760-4.

12. Perlman, S.; Netland, J. Coronaviruses post-SARS: Update on replication and pathogenesis. *Nat. Rev. Microbiol.* **2009**, *7*, 439–450, doi:10.1038/nrmicro2147.

13. Hoffmann, M.; Kleine-Weber, H.; Schroeder, S.; Krüger, N.; Herrler, T.; Erichsen, S.; Schiergens, T.S.; Herrler, G.; Wu, N.H.; Nitsche, A.; et al. SARS-CoV-2 Cell Entry Depends on ACE2 and TMPRSS2 and Is Blocked by a Clinically Proven Protease Inhibitor. *Cell* **2020**, *181*, 271-280.e8, doi:10.1016/j.cell.2020.02.052.

14. Harrison, A.G.; Lin, T.; Wang, P. Mechanisms of SARS-CoV-2 Transmission and Pathogenesis. *Trends Immunol.* **2020**, *41*, 1100–1115, doi:10.1016/j.it.2020.10.004.

15. Shang, J.; Ye, G.; Shi, K.; Wan, Y.; Luo, C.; Aihara, H.; Geng, Q.; Auerbach, A.; Li, F. Structural basis of receptor recognition by SARS-CoV-2. *Nature* **2020**, *581*, 221–224, doi:10.1038/s41586-020-2179-y.

16. Glycoprotein, C.-S.; Walls, A.C.; Park, Y.; Tortorici, M.A.; Wall, A.; Mcguire, A.T.; Veesler, D.; Walls, A.C.; Park, Y.; Tortorici, M.A.; et al. Structure , Function , and Antigenicity of the SARS-CoV-2 Spike Glycoprotein. *Cell* **2020**, *181*, 281-292.e6.

17. Wrobel, A.G.; Benton, D.J.; Xu, P.; Roustan, C.; Martin, S.R.; Rosenthal, P.B.; Skehel, J.J.; Gamblin, S.J. SARS-CoV-2 and bat RaTG13 spike glycoprotein structures inform on virus evolution and furin-cleavage effects. *Nat. Struct. Mol. Biol.* **2020**, *27*, 763–767, doi:10.1038/s41594-020-0468-7.

18. Benton, D.J.; Wrobel, A.G.; Xu, P.; Roustan, C.; Martin, S.R.; Rosenthal, P.B.; Skehel, J.J.; Gamblin, S.J. Receptor binding and priming of the spike protein of SARS-CoV-2 for membrane fusion. *Nature* **2020**, *588*, 327–330, doi:10.1038/s41586-020-2772-0.

19. Kumar, S.; Tharappel, A.M.; Li, Z.; Li, H. Since January 2020 Elsevier has

created a COVID-19 resource centre with free information in English and Mandarin on the novel coronavirus COVID- 19 . The COVID-19 resource centre is hosted on Elsevier Connect , the company ' s public news and information . **2020**.

20. Mckee, D.L.; Sternberg, A.; Stange, U.; Laufer, S.; Naujokat, C.; Millet, J.K.; Whittaker, G.R.; Luan, J.; Lu, Y.; Jin, X.; et al. Since January 2020 Elsevier has created a COVID-19 resource centre with free information in English and Mandarin on the novel coronavirus COVID- 19 . The COVID-19 resource centre is hosted on Elsevier Connect , the company ' s public news and information . **2020**.

21. Gheblawi, M.; Wang, K.; Viveiros, A.; Nguyen, Q.; Zhong, J.C.; Turner, A.J.; Raizada, M.K.; Grant, M.B.; Oudit, G.Y. Angiotensin-Converting Enzyme 2: SARS-CoV-2 Receptor and Regulator of the Renin-Angiotensin System: Celebrating the 20th Anniversary of the Discovery of ACE2. *Circ. Res.* **2020**, 1456–1474, doi:10.1161/CIRCRESAHA.120.317015.

22. Verta, R.; Grange, C.; Skovronova, R.; Tanzi, A.; Peruzzi, L.; Deregibus, M.C.; Camussi, G.; Bussolati, B. Generation of Spike-Extracellular Vesicles (S-EVs) as a Tool to Mimic SARS-CoV-2 Interaction with Host Cells. *Cells* **2022**, *11*, 1–16, doi:10.3390/cells11010146.

23. Bourgonje, A.R.; Abdulle, A.E.; Timens, W.; Hillebrands, J.L.; Navis, G.J.; Gordijn, S.J.; Bolling, M.C.; Dijkstra, G.; Voors, A.A.; Osterhaus, A.D.M.E.; et al. Angiotensin-converting enzyme 2 (ACE2), SARS-CoV-2 and the pathophysiology of coronavirus disease 2019 (COVID-19). *J. Pathol.* **2020**, *251*, 228–248, doi:10.1002/path.5471.

24. Scialo, F.; Daniele, A.; Amato, F.; Pastore, L.; Matera, M.G.; Cazzola, M.; Castaldo, G.; Bianco, A. ACE2: The Major Cell Entry Receptor for SARS-CoV-2. *Lung* **2020**, *198*, 867–877, doi:10.1007/s00408-020-00408-4.

25. Batah, S.S.; Fabro, A.T. Since January 2020 Elsevier has created a COVID-19 resource centre with free information in English and Mandarin on the novel coronavirus COVID- 19 . The COVID-19 resource centre is hosted on Elsevier Connect , the company ' s public news and information . **2020**.

26. Yuan, Y.; Jiao, B.; Qu, L.; Yang, D.; Liu, R. The development of COVID-19 treatment. *Front. Immunol.* **2023**, *14*, 1–13, doi:10.3389/fimmu.2023.1125246.

27. Sreepadmanabh, M.; Sahu, A.K.; Chande, A. COVID-19: Advances in diagnostic tools, treatment strategies, and vaccine development. *J. Biosci.* **2020**, *45*, 1–20, doi:10.1007/s12038-020-00114-6.

28. Grange, C.; Skovronova, R.; Marabese, F.; Bussolati, B. Stem Cell-Derived Extracellular Vesicles and Kidney Regeneration. *Cells* **2019**, *8*, 1–13, doi:10.3390/cells8101240.

29. Van Niel, G.; D'Angelo, G.; Raposo, G. Shedding light on the cell biology of extracellular vesicles. *Nat. Rev. Mol. Cell Biol.* **2018**, *19*, 213–228, doi:10.1038/nrm.2017.125.

30. Grange, C.; Bussolati, B. Extracellular vesicles in kidney disease. *Nat. Rev. Nephrol.* **2022**, *18*, 499–513, doi:10.1038/s41581-022-00586-9.

31. Yokoi, A.; Ochiya, T. Exosomes and extracellular vesicles: Rethinking the essential values in cancer biology. *Semin. Cancer Biol.* **2021**, *74*, 79–91, doi:10.1016/j.semcancer.2021.03.032.

32. Pocsfalvi, G.; Mammadova, R.; Ramos Juarez, A.P.; Bokka, R.; Trepiccione, F.; Capasso, G. COVID-19 and Extracellular Vesicles: An Intriguing Interplay. *Kidney Blood Press. Res.* **2020**, doi:10.1159/000511402.

33. Urbanelli, L.; Buratta, S.; Tancini, B.; Sagini, K.; Delo, F.; Porcellati, S.; Emiliani, C. The role of extracellular vesicles in viral infection and transmission. *Vaccines* **2019**, *7*, 1–20, doi:10.3390/vaccines7030102.

34. Colombo, M.; Raposo, G.; Théry, C. Biogenesis, secretion, and intercellular interactions of exosomes and other extracellular vesicles. *Annu. Rev. Cell Dev. Biol.* **2014**, *30*, 255–289, doi:10.1146/annurev-cellbio-101512-122326.

35. Yáñez-Mó, M.; Siljander, P.R.M.; Andreu, Z.; Zavec, A.B.; Borràs, F.E.; Buzas, E.I.; Buzas, K.; Casal, E.; Cappello, F.; Carvalho, J.; et al. Biological properties of extracellular vesicles and their physiological functions. *J. Extracell. Vesicles* **2015**, *4*, 1–60, doi:10.3402/jev.v4.27066.

36. Chahar, H.S.; Bao, X.; Casola, A. Exosomes and their role in the life cycle and

pathogenesis of RNA viruses. *Viruses* **2015**, *7*, 3204–3225, doi:10.3390/v7062770.

37. Feng, Z., Hensley, L., McKnight, K. L., Hu, F., Madden, V., Ping, L., Jeong, S. H., Walker, C., Lanford, R. E., & Lemon, S.M. A pathogenic picornavirus acquire an envelope by hijacking cellular membranes. *Nature* **2013**, *496*, 367–371.

38. Bukong, T.N.; Momen-Heravi, F.; Kodys, K.; Bala, S.; Szabo, G. Exosomes from Hepatitis C Infected Patients Transmit HCV Infection and Contain Replication Competent Viral RNA in Complex with Ago2-miR122-HSP90. *PLoS Pathog.* **2014**, *10*, doi:10.1371/journal.ppat.1004424.

39. Yan, Y.Y.; Zhou, W.M.; Wang, Y.Q.; Guo, Q.R.; Zhao, F.X.; Zhu, Z.Y.; Xing, Y.X.; Zhang, H.Y.; Aljofan, M.; Jarrahi, A.M.; et al. The Potential Role of Extracellular Vesicles in COVID-19 Treatment: Opportunity and Challenge. *Front. Mol. Biosci.* **2021**, *8*, 1–15, doi:10.3389/fmolb.2021.699929.

40. Yoshikawa, F.S.Y.; Teixeira, F.M.E.; Sato, M.N.; Oliveira, L.M.D.S. Delivery of microrna s by extracellular vesicles in viral infections: Could the news be packaged? *Cells* **2019**, *8*, doi:10.3390/cells8060611.

41. Krishnamachary, B.; Cook, C.; Kumar, A.; Spikes, L.; Chalise, P.; Dhillon, N.K. Extracellular vesicle-mediated endothelial apoptosis and EV-associated proteins correlate with COVID-19 disease severity. *J. Extracell. Vesicles* **2021**, *10*, doi:10.1002/jev2.12117.

42. Balbi, C.; Burrello, J.; Bolis, S.; Lazzarini, E.; Biemmi, V.; Pianezzi, E.; Burrello, A.; Caporali, E.; Grazioli, L.G.; Martinetti, G.; et al. Circulating extracellular vesicles are endowed with enhanced procoagulant activity in SARS-CoV-2 infection. *EBioMedicine* **2021**, *67*, 103369, doi:10.1016/j.ebiom.2021.103369.

43. Liang, B.; Chen, J.; Li, T.; Wu, H.; Yang, W.; Li, Y.; Li, J.; Yu, C.; Nie, F.; Ma, Z.; et al. Clinical remission of a critically ill COVID-19 patient treated by human umbilical cord mesenchymal stem cells: A case report. *Medicine (Baltimore).* **2020**, *99*, e21429, doi:10.1097/MD.0000000000021429.

44. Bari, E.; Ferrarotti, I.; Torre, M.L.; Corsico, A.G.; Perteghella, S. Mesenchymal stem/stromal cell secretome for lung regeneration: The long way through “pharmaceuticalization” for the best formulation. *J. Control. Release* **2019**, *309*,

11–24, doi:10.1016/j.jconrel.2019.07.022.

45. Laffey, J.G.; Matthay, M.A. Cell-based therapy for acute respiratory distress syndrome: Biology and potential therapeutic value. *Am. J. Respir. Crit. Care Med.* **2017**, *196*, 266–273, doi:10.1164/rccm.201701-0107CP.

46. Cocozza, F.; Névo, N.; Piovesana, E.; Lahaye, X.; Buchrieser, J.; Schwartz, O.; Manel, N.; Tkach, M.; Théry, C.; Martin-Jaular, L. Extracellular vesicles containing ACE2 efficiently prevent infection by SARS-CoV-2 Spike protein-containing virus. *J. Extracell. Vesicles* **2020**, *10*, doi:10.1002/jev2.12050.

47. Zhang, J.; Huang, F.; Xia, B.; Yuan, Y.; Yu, F.; Wang, G.; Chen, Q.; Wang, Q.; Li, Y.; Li, R.; et al. The interferon-stimulated exosomal hACE2 potently inhibits SARS-CoV-2 replication through competitively blocking the virus entry. *Signal Transduct. Target. Ther.* **2021**, *6*, 1–11, doi:10.1038/s41392-021-00604-5.

48. Wan, Y.; Shang, J.; Graham, R.; Baric, R.S.; Li, F. Receptor Recognition by the Novel Coronavirus from Wuhan: an Analysis Based on Decade-Long Structural Studies of SARS Coronavirus. *J. Virol.* **2020**, *94*, 1–9, doi:10.1128/jvi.00127-20.

49. Fu, Y.; Xiong, S. Tagged extracellular vesicles with the RBD of the viral spike protein for delivery of antiviral agents against SARS-COV-2 infection. *J. Control. Release* **2021**, *335*, 584–595, doi:10.1016/j.jconrel.2021.05.049.

50. György, B.; Hung, M.E.; Breakefield, X.O.; Leonard, J.N. Therapeutic applications of extracellular vesicles: Clinical promise and open questions. *Annu. Rev. Pharmacol. Toxicol.* **2015**, *55*, 439–464, doi:10.1146/annurev-pharmtox-010814-124630.

51. Scott, T.A.; Supramaniam, A.; Idris, A.; Cardoso, A.A.; Shrivastava, S.; Kelly, G.; Grepo, N.A.; Soemardy, C.; Ray, R.M.; McMillan, N.A.J.; et al. Engineered extracellular vesicles directed to the spike protein inhibit SARS-CoV-2. *Mol. Ther. Methods Clin. Dev.* **2022**, *24*, 355–366, doi:10.1016/j.omtm.2022.01.015.

52. Dudkiewicz, I.; Brosh, T.; Perelman, M.; Salai, M. Colchicine inhibits fracture union and reduces bone strength - In vivo study. *J. Orthop. Res.* **2005**, *23*, 877–881, doi:10.1016/j.orthres.2004.11.014.

53. Dhyani, P.; Quispe, C.; Sharma, E.; Bahukhandi, A.; Sati, P.; Attri, D.C.; Szopa, A.; Sharifi-Rad, J.; Docea, A.O.; Mardare, I.; et al. Anticancer potential of

alkaloids: a key emphasis to colchicine, vinblastine, vincristine, vindesine, vinorelbine and vincamine. *Cancer Cell Int.* **2022**, *22*, 1–20, doi:10.1186/s12935-022-02624-9.

54. Lin, Z.Y.; Kuo, C.H.; Wu, D.C.; Chuang, W.L. Anticancer effects of clinically acceptable colchicine concentrations on human gastric cancer cell lines. *Kaohsiung J. Med. Sci.* **2016**, *32*, 68–73, doi:10.1016/j.kjms.2015.12.006.

55. Marshall M. Kaplan, M.D., David W. Alling, M.D., Ph.D., Hyman J. Zimmerman, M.D., Hubert J. Wolfe, M.D., Robert A. Sepersky, M.D., Gary S. Hirsch, M.D., Grace H. Elta, M.D., Kenneth A. Glick, M.D., and Kathleen A. Eagen, M.D. A Prospective trial of Colchicine for Primary Biliary Cirrhosis. *N. Engl. J. Med.* **1986**, 1448–1454.

56. Zhang, T.; Chen, W.; Jiang, X.; Liu, L.; Wei, K.; Du, H.; Wang, H.; Li, J. Anticancer effects and underlying mechanism of Colchicine on human gastric cancer cell lines in vitro and in vivo. *Biosci. Rep.* **2019**, *39*, 1–10, doi:10.1042/BSR20181802.

57. Toro-Huamanchumo, C.J.; Benites-Meza, J.K.; Mamani-García, C.S.; Bustamante-Paytan, D.; Gracia-Ramos, A.E.; Diaz-Vélez, C.; Barboza, J.J. Efficacy of Colchicine in the Treatment of COVID-19 Patients: A Systematic Review and Meta-Analysis. *J. Clin. Med.* **2022**, *11*, doi:10.3390/jcm11092615.

58. Farhad Salehzadeh, F.P.; Ataei, S. The Impact of Colchicine on COVID-19 patients: A Clinical Trial Study. *Mediterr. J. Rheumatol.* **2022**, *33*, 232–236.

59. Yasmin, F.; Najeeb, H.; Moeed, A.; Hassan, W.; Khatri, M.; Asghar, M.S.; Naveed, A.K.; Ullah, W.; Surani, S. Safety and efficacy of colchicine in COVID-19 patients: A systematic review and meta-analysis of randomized control trials. *PLoS One* **2022**, *17*, 1–13, doi:10.1371/journal.pone.0266245.

60. Cocchi, E.; Chiale, F.; Gianoglio, B.; Deorsola, L.; Napoleone, C.P.; Fagioli, F.; Peruzzi, L. Colchicine: An impressive effect on posttransplant capillary leak syndrome and renal failure. *Pediatrics* **2019**, *143*, doi:10.1542/peds.2018-2820.

61. Cho, J.H.; Joo, Y.H.; Shin, E.Y.; Park, E.J.; Kim, M.S. Anticancer effects of colchicine on hypopharyngeal cancer. *Anticancer Res.* **2017**, *37*, 6269–6280, doi:10.21873/anticanres.12078.

62. Oh, J.; An, H.; Yeo, H.J.; Choi, S.; Oh, J.; Kim, S.; Kim, J.M.; Choi, J.; Lee, S. Colchicine as a novel drug for the treatment of osteosarcoma through drug repositioning based on an FDA drug library. *Front. Oncol.* **2022**, *12*, 1–11, doi:10.3389/fonc.2022.893951.

63. Bussolati, B.; Deambrosis, I.; Russo, S.; Deregibus, M.C.; Camussi, G. Altered angiogenesis and survival in human tumor-derived endothelial cells. *FASEB J.* **2003**, *17*, 1159–1161, doi:10.1096/fj.02-0557fje.

64. Brossa, A.; Buono, L.; Bussolati, B. Effect of the monoclonal antibody TRC105 in combination with Sunitinib on renal tumor derived endothelial cells. *Oncotarget* **2018**, *9*, 22680–22692, doi:10.18632/oncotarget.25206.

65. Brossa, A.; Grange, C.; Mancuso, L.; Annaratone, L.; Satolli, M.A.; Mazzone, M.; Camussi, G.; Bussolati, B. Sunitinib but not VEGF blockade inhibits cancer stem cell endothelial differentiation. *Oncotarget* **2015**, *6*, 11295–11309, doi:10.18632/oncotarget.3123.

66. Veglia, E.; Grange, C.; Pini, A.; Moggio, A.; Lanzi, C.; Camussi, G.; Chazot, P.L.; Rosa, A.C. Histamine receptor expression in human renal tubules: a comparative pharmacological evaluation. *Inflamm. Res.* **2015**, *64*, 261–270, doi:10.1007/s00011-015-0807-z.

67. Kim, J.H.; Lee, K.J.; Seo, Y.; Kwon, J.H.; Yoon, J.P.; Kang, J.Y.; Lee, H.J.; Park, S.J.; Hong, S.P.; Cheon, J.H.; et al. Effects of metformin on colorectal cancer stem cells depend on alterations in glutamine metabolism. *Sci. Rep.* **2018**, *8*, 1–13, doi:10.1038/s41598-017-18762-4.

68. Brossa, A.; Fonsato, V.; Grange, C.; Tritta, S.; Tapparo, M.; Calvetti, R.; Cedrino, M.; Fallo, S.; Gontero, P.; Camussi, G.; et al. Extracellular vesicles from human liver stem cells inhibit renal cancer stem cell-derived tumor growth in vitro and in vivo. *Int. J. Cancer* **2020**, *147*, 1694–1706, doi:10.1002/ijc.32925.

69. Li, B.; Chen, D.; Li, W.; Xiao, D. 20(S)-protopanaxadiol saponins inhibit SKOV3 cell migration. *Oncol. Lett.* **2016**, *11*, 1693–1698, doi:10.3892/ol.2016.4155.

70. Paba, C.; Dorigo, V.; Senigagliesi, B.; Tormena, N.; Parisse, P.; Voitchovsky, K.; Casalis, L. Lipid bilayer fluidity and degree of order regulates small EVs adsorption on model cell membrane. *J. Colloid Interface Sci.* **2023**, *652*, 1937–

1943, doi:10.1016/j.jcis.2023.08.117.

71. Rampino, T.; Gregorini, M.; Guidetti, C.; Broggini, M.; Marchini, S.; Bonomi, R.; Maggio, M.; Roscini, E.; Soccio, G.; Tiboldo, R.; et al. KCNA1 and TRPC6 ion channels and NHE1 exchanger operate the biological outcome of HGF/scatter factor in renal tubular cells. *Growth Factors* **2007**, *25*, 382–391, doi:10.1080/08977190801892184.

72. Paduano, F.; Marrelli, M.; Palmieri, F.; Tatullo, M. CD146 Expression Influences Periapical Cyst Mesenchymal Stem Cell Properties. *Stem Cell Rev. Reports* **2016**, *12*, 592–603, doi:10.1007/s12015-016-9674-4.

73. Togarrati, P.P.; Dinglasan, N.; Desai, S.; Ryan, W.R.; Muench, M.O. CD29 is highly expressed on epithelial, myoepithelial, and mesenchymal stromal cells of human salivary glands. *Oral Dis.* **2018**, *24*, 561–572, doi:10.1111/odi.12812.

74. Cai, Y., Zhang, J., Xiao, T., Peng, H., Sterling, S. M., Walsh, R. M., Jr, Rawson, S., Rits-Volloch, S., & Chen, B. Distinct conformaational states of SARS-CoV-2 spike protein. *Science (80-.).* **2020**, *369*, 1586–1592.

75. Jin, Y.; Ji, W.; Yang, H.; Chen, S.; Zhang, W.; Duan, G. Endothelial activation and dysfunction in COVID-19: from basic mechanisms to potential therapeutic approaches. *Signal Transduct. Target. Ther.* **2020**, *5*, 1–13, doi:10.1038/s41392-020-00454-7.

76. Amraei, R.; Rahimi, N. COVID-19, Renin-Angiotensin System and Endothelial Dysfunction. *Cells* **2020**, *9*, 1–18, doi:10.3390/cells9071652.

77. Liao, Y.; Li, X.; Mou, T.; Zhou, X.; Li, D.; Wang, L.; Zhang, Y.; Dong, X.; Zheng, H.; Guo, L.; et al. Distinct infection process of SARS-CoV-2 in human bronchial epithelial cell lines. *J. Med. Virol.* **2020**, *92*, 2830–2838, doi:10.1002/jmv.26200.

78. Asahina, A.; Tada, Y.; Nakamura, K.; Tamaki, K. Colchicine and griseofulvin inhibit VCAM-1 expression on human vascular endothelial cells - Evidence for the association of VCAM-1 expression with microtubules. *J. Dermatol. Sci.* **2001**, *25*, 1–9, doi:10.1016/S0923-1811(00)00097-9.

79. Dasgeb, B.; Kornreich, D.; McGuinn, K.; Okon, L.; Brownell, I.; Sackett, D.L. Colchicine: an ancient drug with novel applications. *Br. J. Dermatol.* **2018**, *178*, 350–356, doi:10.1111/bjd.15896.

80. Grange, C.; Tapparo, M.; Collino, F.; Vitillo, L.; Damasco, C.; Deregibus, M.C.; Tetta, C.; Bussolati, B.; Camussi, G. Microvesicles released from human renal cancer stem cells stimulate angiogenesis and formation of lung premetastatic niche. *Cancer Res.* **2011**, *71*, 5346–5356, doi:10.1158/0008-5472.CAN-11-0241.

81. Wen-Hsuan Chang, Richard A Cerione, M.A.A. Extracellular Vesicles and Their Roles in Cancer Progression. *Methods Mol. Biol.* **2021**, *2174*, 143–170.

82. Ye, Z.W.; Yu, Z.L.; Chen, G.; Jia, J. Extracellular vesicles in tumor angiogenesis and resistance to anti-angiogenic therapy. *Cancer Sci.* **2023**, *114*, 2739–2749, doi:10.1111/cas.15801.

83. Fleming, A.; Sampey, G.; Chung, M.C.; Bailey, C.; van Hoek, M.L.; Kashanchi, F.; Hakami, R.M. The carrying pigeons of the cell: Exosomes and their role in infectious diseases caused by human pathogens. *Pathog. Dis.* **2014**, *71*, 109–120, doi:10.1111/2049-632X.12135.

84. Han, L.; Lam, E.W.F.; Sun, Y. Extracellular vesicles in the tumor microenvironment: Old stories, but new tales. *Mol. Cancer* **2019**, *18*, 1–14, doi:10.1186/s12943-019-0980-8.

85. Owczarek, K.; Szczepanski, A.; Milewska, A.; Baster, Z.; Rajfur, Z.; Sarna, M.; Pyrc, K. Early events during human coronavirus OC43 entry to the cell. *Sci. Rep.* **2018**, *8*, 1–12, doi:10.1038/s41598-018-25640-0.

86. Wang, J.; Chen, S.; Bihl, J. Exosome-Mediated Transfer of ACE2 (Angiotensin-Converting Enzyme 2) from Endothelial Progenitor Cells Promotes Survival and Function of Endothelial Cell. *Oxid. Med. Cell. Longev.* **2020**, *2020*, doi:10.1155/2020/4213541.

87. Kaul, D. Since January 2020 Elsevier has created a COVID-19 resource centre with free information in English and Mandarin on the novel coronavirus COVID-19 . The COVID-19 resource centre is hosted on Elsevier Connect , the company ' s public news and information . **2020**.

88. Chai, P.; Yu, J.; Ge, S.; Jia, R.; Fan, X. Genetic alteration, RNA expression, and DNA methylation profiling of coronavirus disease 2019 (COVID-19) receptor ACE2 in malignancies: A pan-cancer analysis. *J. Hematol. Oncol.* **2020**, *13*, 1–

5, doi:10.1186/s13045-020-00883-5.

89. Troyer, Z.; Alhusaini, N.; Tabler, C.O.; Sweet, T.; Carvalho, K.I.L.; Schlatzer, D.M.; Carias, L.; King, C.L.; Matreyek, K.; Tilton, J.C. Extracellular vesicles carry SARS-CoV-2 spike protein and serve as decoys for neutralizing antibodies. *J. Extracell. Vesicles* **2021**, *10*, doi:10.1002/jev2.12112.

90. Baden, L.R.; El Sahly, H.M.; Essink, B.; Kotloff, K.; Frey, S.; Novak, R.; Diemert, D.; Spector, S.A.; Rouphael, N.; Creech, C.B.; et al. Efficacy and Safety of the mRNA-1273 SARS-CoV-2 Vaccine. *N. Engl. J. Med.* **2021**, *384*, 403–416, doi:10.1056/nejmoa2035389.

91. Teo, S.P. Review of COVID-19 mRNA Vaccines: BNT162b2 and mRNA-1273. *J. Pharm. Pract.* **2022**, *35*, 947–951, doi:10.1177/08971900211009650.

92. Bansal, S.; Perincheri, S.; Fleming, T.; Poulson, C.; Tiffany, B.; Bremner, R.M.; Mohanakumar, T. Cutting Edge: Circulating Exosomes with COVID Spike Protein Are Induced by BNT162b2 (Pfizer–BioNTech) Vaccination prior to Development of Antibodies: A Novel Mechanism for Immune Activation by mRNA Vaccines. *J. Immunol.* **2021**, *207*, 2405–2410, doi:10.4049/jimmunol.2100637.

93. Luchini, A.; Micciulla, S.; Corucci, G.; Batchu, K.C.; Santamaria, A.; Laux, V.; Darwish, T.; Russell, R.A.; Thepaut, M.; Bally, I.; et al. Lipid bilayer degradation induced by SARS-CoV-2 spike protein as revealed by neutron reflectometry. *Sci. Rep.* **2021**, *11*, 1–11, doi:10.1038/s41598-021-93996-x.

94. Asandei, A.; Mereuta, L.; Schiopu, I.; Park, J.; Seo, C.H.; Park, Y.; Luchian, T. Non-Receptor-Mediated Lipid Membrane Permeabilization by the SARS-CoV-2 Spike Protein S1 Subunit. *ACS Appl. Mater. Interfaces* **2020**, *12*, 55649–55658, doi:10.1021/acsami.0c17044.

95. Guillén, J.; De Almeida, R.F.M.; Prieto, M.; Villalaín, J. Structural and dynamic characterization of the interaction of the putative fusion peptide of the S2 SARS-CoV virus protein with lipid membranes. *J. Phys. Chem. B* **2008**, *112*, 6997–7007, doi:10.1021/jp7118229.

96. Palacios-Rápalo, S.N.; De Jesús-González, L.A.; Cordero-Rivera, C.D.; Farfan-Morales, C.N.; Osuna-Ramos, J.F.; Martínez-Mier, G.; Quistián-Galván, J.;

Muñoz-Pérez, A.; Bernal-Dolores, V.; del Ángel, R.M.; et al. Cholesterol-Rich Lipid Rafts as Platforms for SARS-CoV-2 Entry. *Front. Immunol.* **2021**, *12*, 1–17, doi:10.3389/fimmu.2021.796855.

97. Wang, H.; Yuan, Z.; Pavel, M.A.; Jablonski, S.M.; Jablonski, J.; Hobson, R.; Valente, S.; Reddy, C.B.; Hansen, S.B. The role of high cholesterol in SARS-CoV-2 infectivity. *J. Biol. Chem.* **2023**, *299*, 104763, doi:10.1016/j.jbc.2023.104763.

98. Correa, Y.; Waldie, S.; Thépaut, M.; Micciula, S.; Moulin, M.; Fieschi, F.; Pichler, H.; Trevor Forsyth, V.; Haertlein, M.; Cárdenas, M. SARS-CoV-2 spike protein removes lipids from model membranes and interferes with the capacity of high density lipoprotein to exchange lipids. *J. Colloid Interface Sci.* **2021**, *602*, 732–739, doi:10.1016/j.jcis.2021.06.056.

99. Liao, Y.; Li, X.; Mou, T.; Zhou, X.; Li, D.; Wang, L.; Zhang, Y.; Dong, X.; Zheng, H.; Guo, L.; et al. Distinct infection process of SARS-CoV-2 in human bronchial epithelial cell lines. *J. Med. Virol.* **2020**, *92*, 2830–2838, doi:10.1002/jmv.26200.

100. Blume, C.; Jackson, C.L.; Spalluto, C.M.; Legebeke, J.; Nazlamova, L.; Conforti, F.; Perotin, J.M.; Frank, M.; Butler, J.; Crispin, M.; et al. A novel ACE2 isoform is expressed in human respiratory epithelia and is upregulated in response to interferons and RNA respiratory virus infection. *Nat. Genet.* **2021**, *53*, 205–214, doi:10.1038/s41588-020-00759-x.

101. Choi, D.; Khan, N.; Montermini, L.; Tawil, N.; Meehan, B.; Kim, D.; Roth, F.P.; Divangahi, M.; Rak, J. Quantitative proteomics and biological activity of extracellular vesicles engineered to express SARS-CoV-2 spike protein. *J. Extracell. Biol.* **2022**, *1*, doi:10.1002/jex2.58.

102. Leung, Y.Y.; Yao Hui, L.L.; Kraus, V.B. Colchicine-Update on mechanisms of action and therapeutic uses. *Semin. Arthritis Rheum.* **2015**, *45*, 341–350, doi:10.1016/j.semarthrit.2015.06.013.

103. Manenti, L.; Maggiore, U.; Fiaccadori, E.; Meschi, T.; Antoni, A.D.; Nouvenne, A.; Ticinesi, A.; Cerundolo, N.; Prati, B.; Delsante, M.; et al. Reduced mortality in COVID-19 patients treated with colchicine: Results from a retrospective, observational study. *PLoS One* **2021**, *16*, 1–11,

doi:10.1371/journal.pone.0248276.

104. Sukeishi, A.; Isami, K.; Hiyama, H.; Imai, S.; Nagayasu, K.; Shirakawa, H.; Nakagawa, T.; Kaneko, S. Colchicine alleviates acute postoperative pain but delays wound repair in mice: Roles of neutrophils and macrophages. *Mol. Pain* **2017**, *13*, 1–12, doi:10.1177/1744806917743680.

105. Bitler, A.; Dover, R.; Shai, Y. Anticancer Drug Colchicine Increases Disorder and Reduces Complexity in the Macrophage Membrane. *Biophys. J.* **2016**, *110*, 83a, doi:10.1016/j.bpj.2015.11.507.

106. Rao, P.; Falk, L.A.; Dougherty, S.F.; Sawada, T.; Pluznik, D.H. Colchicine Down-Regulates Lipopolysaccharide-Induced Granulocyte-Macrophage Colony-Stimulating Factor Production in Murine Macrophages. *J. Immunol.* **1997**, *159*, 3531–3539.

107. Demidowich, A.P.; Davis, A.I.; Dedhia, N.; Yanovski, J.A. Colchicine to decrease NLRP3-activated inflammation and improve obesity-related metabolic dysregulation. *Med. Hypotheses* **2016**, *92*, 67–73, doi:10.1016/j.mehy.2016.04.039.

108. Martínez, G.J.; Celermajer, D.S.; Patel, S. The NLRP3 inflammasome and the emerging role of colchicine to inhibit atherosclerosis-associated inflammation. *Atherosclerosis* **2018**, *269*, 262–271, doi:10.1016/j.atherosclerosis.2017.12.027.

109. Bai, B.; Yang, Y.; Wang, Q.; Li, M.; Tian, C.; Liu, Y.; Aung, L.H.H.; Li, P. feng; Yu, T.; Chu, X. ming NLRP3 inflammasome in endothelial dysfunction. *Cell Death Dis.* **2020**, *11*, doi:10.1038/s41419-020-02985-x.

110. An, N.; Gao, Y.; Si, Z.; Zhang, H.; Wang, L.; Tian, C.; Yuan, M.; Yang, X.; Li, X.; Shang, H.; et al. Regulatory mechanisms of the NLRP3 inflammasome, a novel immune-inflammatory marker in cardiovascular diseases. *Front. Immunol.* **2019**, *10*, 1–11, doi:10.3389/fimmu.2019.01592.